Hydrogen Gas Sensors Using Palladium Nanogaps on an Elastomeric Substrate

Hyun-Sook Lee, Jeongmin Kim, Hongjae Moon, and Wooyoung Lee*

With the recent reillumination of the hydrogen economy around the world, the demand for H_2 sensors is expected to increase rapidly. Due to safety issues caused by the highly flammable and explosive character of hydrogen gas (H_2), it is imperative to develop the sensors that can quickly and sensitively detect H_2 leaks. For the development of H_2 sensors, Pd-based materials have been extensively used due to the high affinity of Pd metal for H_2. Among Pd-based H_2 sensors, Pd nanogap-based sensors have been extensively investigated because these sensors can operate in an on–off manner, which enables them to have improved sensing capabilities, including high sensitivity, rapid response, short recovery time, and good reliability. Importantly, significant advances in H_2-sensing performance have been achieved by simply using an elastomeric substrate to form Pd nanogaps. Herein, the progress and advanced approaches achieved over the last decade for Pd nanogap-based H_2 sensors supported on elastomeric substrates are reviewed, with a focus on strategies to reduce detection limits and increase reliability, sensitivity, and stability.

1. Introduction

1.1. Hydrogen Sensors

H_2 has been regarded as an eco-friendly and efficient energy source for decades owing to its cleanliness, abundance, and recyclability. However, it has a wide explosive concentration range (4–75 vol%), high heat of combustion (142 kJ g^{-1}), low ignition energy (0.02 mJ), and high flame propagation velocity.[1] Moreover, H_2 gas is colorless, odorless, and tasteless; hence, it cannot be sensed by humans. Therefore, accurate and rapid detection of H_2 is an essential prerequisite for its widespread use in a variety of fields. This requirement has led to extensive research on the development of high-performance H_2 sensors. In particular, the number of studies related to H_2 sensors has increased significantly since 2000, as shown in the graph of **Figure 1**. Consequently, various types of H_2 sensors have been proposed and practically used.[2–10] The commercially available sensors that

Dr. H.-S. Lee, Dr. H. Moon, Prof. W. Lee
Department of Materials Science and Engineering
Yonsei University
50 Yonsei-ro, Seodaemoon-gu, Seoul 03722, Republic of Korea
E-mail: wooyoung@yonsei.ac.k
Dr. J. Kim
Division of Nanotechnology
DGIST
333 Techno Jungang-daero, Hyeonpung-eup, Dalseong-gun, Daegu 42988, Republic of Korea

The ORCID identification number(s) for the author(s) of this article can be found under https://doi.org/10.1002/adma.202005929.

utilize different sensing mechanisms and their performance specifications are presented in **Table 1**.[1] (These data were obtained from the summary of a survey that was recently conducted by Hübert et al.[1]) In addition, the global demand for gas sensors continues to increase: the global Gas Sensor Market was valued at $2.54 billion in 2017 and is expected to reach $3.7 billion in global sales by 2025 (https://www.ameriresearch.com/product/gas-sensor-market/). Therefore, the global H_2 gas-sensor market will also grow significantly in fields where H_2 is produced, stored, distributed, or used.

1.2. Pd-Based H_2 Gas Detection

Among H_2 sensors, Pd-based sensors have been widely studied because of the inherent ability of Pd to easily dissociate H_2 molecules into H atoms on the Pd surface and then spontaneously and selectively absorb H atoms in octahedral interstitial sites of the face-centered cubic (fcc) Pd lattice at room temperature.[11–14] With the developments in microstructure technology, it is possible to improve the electrical H_2-sensing performance by imprinting-based Pd grating and a crackle lithography-based Pd network,[15,16] and H_2 detection based on changes in optical properties has been demonstrated.[17]

Among Pd-based H_2 sensors, Pd nanogap-based H_2 sensors, which operate in an on–off manner, exhibit excellent sensing performance, including high sensitivity, rapid response, short recovery time, and good reliability.[18] This is a novel approach to overcome the problems inherent in the scalability of Pd nanowire H_2 sensors and the poor sensing properties of Pd-thin film H_2 sensors. In Pd nanogap-based H_2 sensors, the nanogap width plays an important role in the H_2 sensing performance. Thus, there have been a variety of approaches to control the width of Pd nanogaps for improved sensing properties.

A Pd H_2 sensor based on nanogaps was first demonstrated using Pd mesowire arrays 20 years ago.[19] Mesowires composed of Pd nanoparticles were electrodeposited on the edge of a step in single-crystalline graphite and were transferred onto a cyanoacrylate film (**Figure 2**a). Up to 100 Pd mesowires were arrayed in parallel, as shown in Figure 2b. The Pd mesowires were initially electrically conductive (Figure 2c). However, after the H_2 exposure cycle, volume shrinkage of the Pd nanoparticles occurred, creating a nanogap between the Pd nanoparticles. As a result, current stopped flowing, making the mesowire an on–off sensor (Figure 2c). The break junction mechanism was confirmed by atomic force microscopy observation of
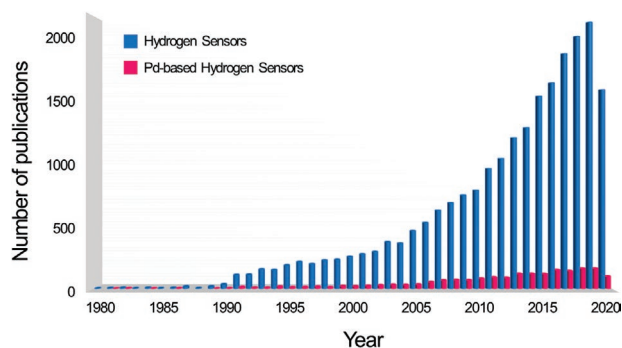
Figure 1. Growth in the number of studies related to H_2 sensors since 1980 according to an enquiry (October 2020) of the ISI Web of Knowledge, Thomson Reuters.

individual Pd mesowires (Figure 2d). The results confirmed that Pd mesowires could substantially improve H_2-sensing performance, but they also revealed a disadvantage for detecting low concentration of H_2, i.e., high detection limit of 2.25%. On the other hand, Pd mesowires can operate as an always-on sensor when the nanoparticles are distributed too densely. The detection limit of the always-on sensor was ≈0.5%. To improve the sensitivity of Pd nanowires, various fabrication methods have been proposed.[20–22] Lithographically patterned nanowire electrodeposition (LPNE) enabled the fabrication of single Pd nanowires with significantly reduced lateral dimensions (reduced to 20 nm in height).[21] The results demonstrated that decreasing the Pd nanowire size led to improved

sensing performance in terms of sensitivity, response time, and recovery time.[21] Moreover, these nanowires could detect H_2 in nitrogen in the range of 2 ppm to 10%.[21] Furthermore, the surface of the Pd nanowires prepared by LPNE was uniformly coated with a Pt layer. The response speed of the Pd–Pt core–shell nanowires was increased by a factor of 2 relative to that of uncoated Pd nanowires, and the recovery time was accelerated by a factor of 25 at the limit of detection in air.[22] The sensing performance of these modified Pd nanowires was strongly affected by temperature. As the operating temperature increased, the response and recovery significantly improved due to thermally activated sensing process, but the sensing response decreased because of the low solubility of H in PdH_x in the heated nanowires.[20–23]

The detection mechanism of this type of Pd mesowire array on single-crystalline graphite step edges is based on the lattice expansion of discontinuous Pd nanoclusters during hydrogenation. The application of the sensing mechanism was expanded to sensors based on discontinuous ultrathin Pd films.[24–28] During exposure to H_2, some clusters form electrical connections because of the Pd volume expansion, and conducting pathways are created through the film, thereby reducing the overall electrical resistance of the film (**Figure 3**). To understand the H_2-sensing behaviors and the corresponding electric transport mechanisms, ultrathin Pd films were investigated using various substrate materials such as SiO_2,[24] Si,[25] Si_3N_4,[26] supporting polymer (SU8),[27] and siloxane self-assembled monolayers (SAMs).[28] Among these materials, a discontinuous ultrathin Pd film deposited on a siloxane SAM-coated glass

Table 1. Comparison of the performance specifications of commercially available sensors. Reproduced with permission.[1] Copyright 2011, Elsevier B.V.

Sensor type	Mechanism	Performance				
		Detection range [vol%]	Response time [s]	Power consumption [mW]	Gas environment	Lifetime [years]
Catalytic	Pellistor	Up to 4	<30	1000	−20 to 70 °C 5–95% RH 70–130 kPa	5
Thermal conductivity	Calorimetric	1–100	<10	<500	0–50 °C 0–95% RH 80–120 kPa	5
Electrochemical	Amperometric	Up to 4	<90	2–700	−20 to 55 °C 5–95% RH 80–110 kPa	2
Resistance-based	Semiconducting metal–oxide	Up to 2	<20	<800	−20 to 70 °C 10–95% RH 80–120 kPa	>2
	Metallic resistor	0.1–100	<15	>25	0–45 °C 0–95% RH Up to 700 kPa	<10
Work function-based	Capacitor	Up to 5	<60	4000	−20 to 40 °C 0–95% RH 80–120 kPa	10
	MOS field effect transistor	Up to 4.4	<2	700	−40 to 110 °C 5–95% RH 70–130 kPa	10
Optical	Optrode	0.1–100	<60	1000	−15 to 50 °C 0–95% RH 75–175 kPa	>2

ADVANCED
SCIENCE NEWS
www.advancedsciencenews.com
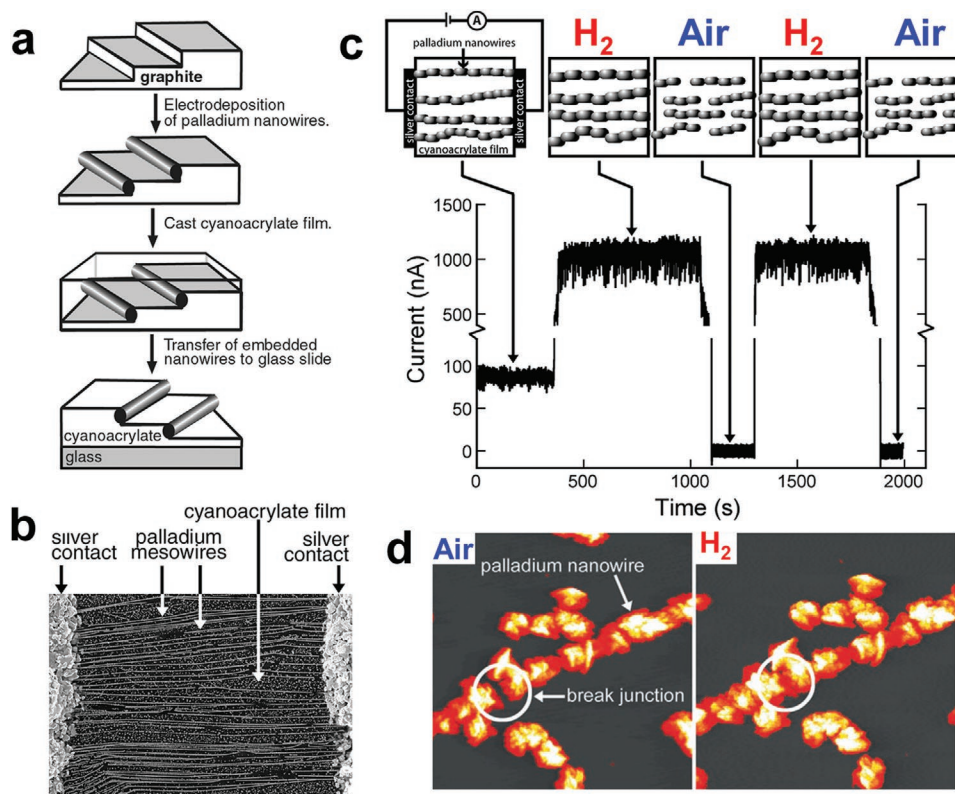
ADVANCED
MATERIALS
www.advmat.de

Figure 2. a) Schematic diagrams of formation procedure of Pd mesowire arrays (PMA). b) Scanning electron microscope (SEM) image of the active area of a PMA-based H_2 sensor. c) Sensing mechanism (top) and current response (bottom) of PMA-based H_2 sensor. d) Atomic force microscope (AFM) images of a Pd mesowire on a graphite surface in air (left) and H_2 (right). A H_2-actuated break junction is highlighted. Reproduced with permission.[19] Copyright 2001, American Association for the Advancement of Science.

substrate showed a rapid response time of 70 ms for 2% H_2 and a low detection limit of 25 ppm H_2.[28] This was explained by the narrowing of the intercluster gaps, which was attributed to the reduction of adhesion between Pd and the glass substrate due to the siloxane SAM.[28]

Nanogap-based H_2 sensors using Pd nanowires have been further studied.[29–33] Pd nanowires were fabricated by electrodeposition with different Pd plating solutions[29–31] or different templates (highly oriented pyrolitic graphite (HOPG))[32] and anodic aluminum oxide nanopore (AAO) films.[33,34] All these sensors operated through the opening and closing of the Pd nanogaps upon exposure to H_2. It has been shown that the

Figure 3. Schematics of the H_2-sensing mechanism in ultrathin Pd films: a) discontinuous and nonconducting Pd nanocluster film before exposure to H_2 and b) formation of conducting pathways due to continuous Pd nanoclusters by volume expansion during exposure to H_2.

sensitivity and response time of the sensors are greatly affected by nanogap formation, which is influenced by the nanowire diameter and surface morphology. In particular, free-standing Pd nanowire arrays were fabricated after electrodepositing into the nanopores of the AAO film and removing the AAO template. The diameter of the nanowires was in the range of 80–90 nm. The nanogap distance between the wires varied greatly across the array, ranging from a few nanometers to hundreds of nanometers, as shown in **Figure 4**. Owing to the high surface area of nanowires, this nanowire array sensor could detect H_2 concentrations as low as 0.2% with rapid response and recovery times of 0.7 and 20 s, respectively.

In addition, a novel fabrication method for Pd-based H_2 sensors with vertical nanogaps has been reported.[35] Vertical nanogaps between two suspended Pd/Ti/poly-Si trimorph electrodes and a single fixed Pd/Ti bottom electrode were demonstrated (**Figure 5**). These sensors can be manufactured on a large scale and have the advantage of significantly reducing the nanogap width to less than 10 nm. However, despite the narrow width of nanogaps, these sensors suffer from a high detection limit of ≈1.5%, similar to that of other nanogap sensors, and they also do not operate in an on–off manner.

In particular, in Pd nanogap-based H_2 sensors, significant advances in H_2-sensing properties have been achieved by simply using an elastomeric substrate to form a cracked Pd thin film, in which the cracks act as nanogaps.[18] This lithography-free method is quite cost-effective and allows for
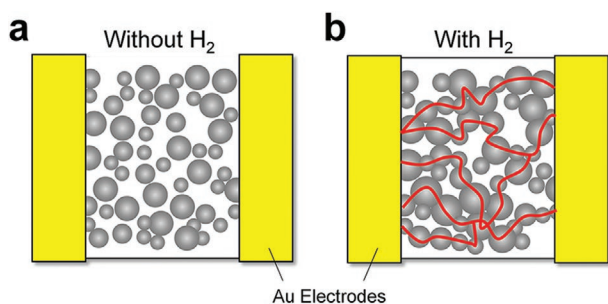
**ADVANCED
SCIENCE NEWS**
www.advancedsciencenews.com
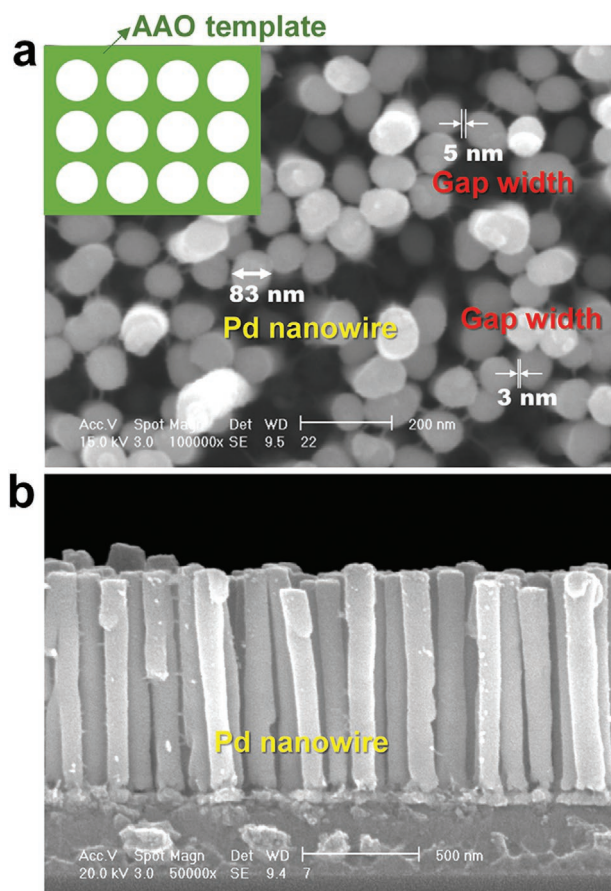
**ADVANCED
MATERIALS**
www.advmat.de

Figure 4. Scanning electron microscope (SEM) images of Pd nanowires grown on Si substrate using AAO template. a) Top-view image of Pd nanowires showing the diameter of nanowires and gaps between nanowires. b) Cross-sectional view of the free-standing Pd nanowires on Si substrate after the removal of AAO template. Reproduced with permission.[34] Copyright 2006, IEEE Xplore.

the manufacture of large-scale devices. Herein, we review the progress and advanced approaches for Pd nanogap-based H_2 sensors supported on elastomeric substrates, which have been achieved over the past decade. This review is classified into the following categories: strategies for reducing detection limits; enhancing reliability, selectivity, and sensitivity; and improving stability in humid and thermal conditions.
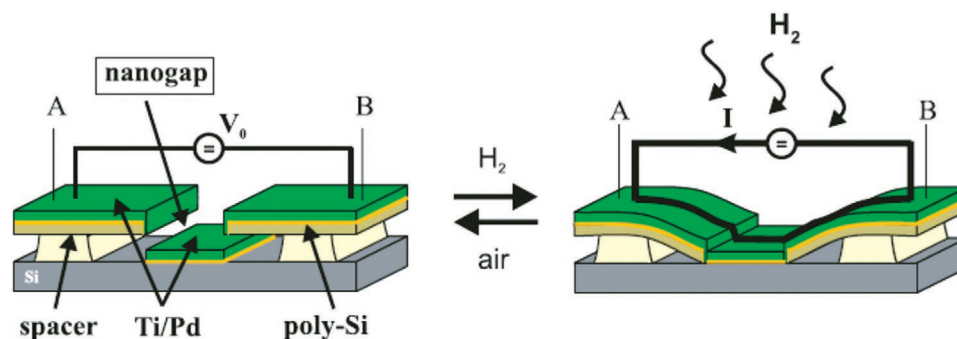
1.3. Historical Review of Pd Nanogap H_2 Sensors on Elastomeric Substrates

Figure 6 summarizes 10 years of extensive research on H_2 gas sensors based on Pd nanogaps formed on elastomeric substrates, aimed at demonstrating the enhancement of H_2 detection performance. In 2011, H_2 sensors based on Pd expansion due to the absorption of H atoms were reported by Lee et al., using nanogaps formed by generating cracks on a Pd film deposited on polydimethylsiloxane (PDMS) with mechanical stretching without a lithography process.[18] This was the first H_2 sensor demonstrated on an elastomeric substrate, in which clear on–off sensing signals were obtained at an H_2 concentration lower than that of other sensors based on the Pd expansion mechanism by implementing highly mobile films, thereby eliminating the stress at the interface due to the volumetric change. Therefore, these H_2 sensors were called highly mobile thin films on elastomers (MOTIFE). The PdNi alloy-based MOTIFEs reported with Pd MOTIFEs showed improved performance, including the rapid response time, high concentration discernibility, and a low concentration detection limit through a study on the optimization of Ni content during the following year (2012).[36] In the same year, a cracked Pd film on an elastomeric substrate (CPE) was developed based on a spontaneous nanogap formation process by absorption and desorption of H_2 without the stretching process.[37] In this work, the reversible on–off sensing mechanism of Pd nanogaps on the elastomer was analyzed in detail through a systematic study of the thickness of Pd films. In 2013, a liquid nitrogen freezing (LNF) process that reduces the H_2 detection limit by decreasing the nanogap width in both Pd MOTIFEs and CPEs was reported.[38] Moreover, by controlling the H_2 exposure during the nanogap formation process, extremely small nanogap widths were obtained, detecting the lowest H_2 concentration ever reported in Pd film-based sensors.[39] Separately, a different approach to decrease the detection limit was also attempted by connecting a Pd MOTIFE with an oxide thin-film transistor (TFT).[40] In this early stage of the study, H_2 sensing tests were conducted in an inert atmosphere with N_2 carrier to investigate the on–off sensing mechanism and to improve the intrinsic sensing performance, including the sensitivity, detection limit, discernibility, and response time.

In subsequent studies, for practical application of H_2 sensors based on Pd nanogaps on elastomeric substrates, the

Figure 5. Schematics of the sensing mechanism based on an interconnection between suspended Pd/Ti/poly-Si top electrodes and a Pd/Ti bottom electrode. Reproduced with permission.[35] Copyright 2010, IOP Publishing Ltd.
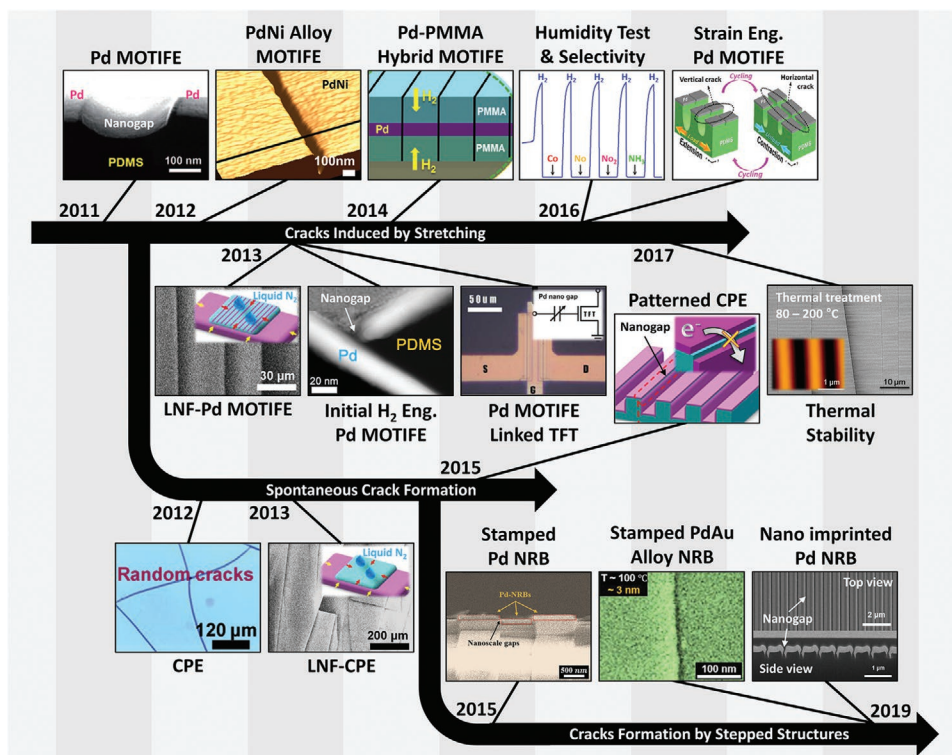
Figure 6. Historical overview of research on H₂ sensors based on Pd nanogaps formed on elastomeric substrates. According to the nanogap formation method, these elastomer-based nanogap sensors are classified into MOTIFEs, where the cracks of Pd films were generated by mechanical stretching; CPEs, which are based on spontaneous cracking of Pd due to H₂ absorption and desorption; and NRBs, in which the cracks were formed by stepped structures. In the early stages, intrinsic H₂ sensing performance including the sensitivity, detection limit, discernibility, and response time were studied in N₂. In the subsequent studies, the sensing properties for practical use were investigated, such as the reliability, stability, and selectivity. Reproduced with permission.[18] Copyright 2011, Wiley-VCH GmbH. Reproduced with permission.[36,37] Copyright 2012, Elsevier B.V. Reproduced with permission.[38,39] Copyright 2013, Elsevier B.V. Reproduced with permission.[40] Copyright 2013, Royal Society of Chemistry. Reproduced with permission.[41] Copyright 2014, Elsevier B.V. Reproduced with permission.[42] Copyright 2015, Elsevier B.V. Reproduced with permission.[43] Copyright 2015, Wiley-VCH GmbH. Reproduced with permission.[44,46] Copyright 2016, Elsevier B.V. Reproduced with permission.[45] Copyright 2016, Springer Nature. Reproduced with permission.[47] Copyright 2017, Elsevier B.V. Reproduced with permission.[48] Copyright 2019, Wiley-VCH GmbH. Reproduced with permission.[49] Copyright 2019, IEEE-INST Electrical Electronics Engineers Inc.

reliability of advanced Pd MOTIFEs and CPEs in ambient atmosphere, stability under humid conditions, selectivity in several toxic gases, and thermal stability were intensively investigated. First, a Pd–polymethyl methacrylate (PMMA) hybrid MOTIFE was developed by Jang et al. in 2014, in which Pd nanogaps were sandwiched by a thin PMMA layer. Hence, the detection limit in air could be reduced by selective penetration of H₂.[41] In addition, improved H₂ sensing performance was demonstrated with a patterned CPE in air based on an artificially controlled Pd grating using the nanoimprint lithography (NIL) technique in the following year (2015).[42] In the same year, a stamped Pd nanoribbon (NRB) array was also developed, which was fabricated using the imprint transfer technique of a Pd film based on a polyethylene terephthalate (PET) substrate.[43] In 2016, it was realized that the detection limit in air could be reduced by controlling the strain parameters, including the strain velocity and magnitude, of the crack generating process using mechanical stretching based on the typical Pd MOTIFE without the development of complex structures.[44,45] In this study, it was clarified that the nanogap density plays an important role in the detection of low H₂ concentration, as does the control of nanogap dimensions

with strain engineering. The degradation of the H₂ sensing signal of Pd MOTIFEs under various humidity conditions was investigated, and the selectivity of H₂ over several toxic gases including CO, NO, NO₂, and NH₃ was also confirmed in the same year.[46] The thermal stability of the Pd MOTIFEs was studied by observing the influence of annealing temperatures from 80 to 200 °C on the H₂ sensing performance in 2017.[47] Pak et al. developed an advanced stamped NRB array in 2019.[48] In this stamped PdAu alloy NRB, the width of the nanogap was controlled by annealing of the polystyrene (PS) substrate, and at the same time, the β Pd hydride formation was suppressed through Au alloying. As a result, the stability of H₂ detection increased dramatically, and a very low detection limit was demonstrated in an air environment. A fabrication method of Pd NRB based on polyurethane acrylate (PUA) substrates was also reported using the nanoimprint technique in 2019.[49] The fabrication process and the sensing performance specifications of various H₂ sensors based on the Pd nanogaps formed on the elastomeric substrates are summarized in **Table 2**. The enhancement of sensing performance caused by variations in each process parameter is discussed in detail in the next section.

Table 2. Comparison of the process and performance specifications of H₂ sensors based on the Pd nanogaps formed on the elastomeric substrates.

	Pd nanogaps on elastomer	Materials	Thickness [nm]	Initial stretching Strain [%]	Initial stretching Velocity [μm s⁻¹]	Temperature [°C]	Initial H₂ exposure [%]	Carrier gas	Gap size [nm]	Detection limit [%]	Discernibility [%]	Response time [s]	Recovery time [s]	Refs.
MOTIFE	Pd MOTIFE	Pd	10	25	–	25	10	N_2	300	0.4	2	0.67	3.36	[18]
			10	25	–		4	N_2	50	0.2	–	–	–	[40]
			10	50	–		0.5	N_2	50	0.01	–	<1	<1	[46]
			12	25	–		2	Air	–	1.2	–	<0.4	<0.4	[41]
	PdNi alloy MOTIFE	93:7	6	25	–	25	10	N_2	–	0.08	>4	0.5	1.68	[18]
		87.5:12.5	10						62	0.01	10	<1	<1	[36]
	LNF-Pd MOTIFE	Pd	10	25	–	25	5	N_2	25	0.02	2	<1	–	[38]
	Initial H₂ eng. Pd MOTIFE	Pd	10	25	–	25	0.1	N_2	8	0.001	0.1	<10	<10	[39]
							1.5		40	0.2	1.5			
							3		>50	0.35	2			
	Pd–PMMA hybrid MOTIFE	PMMA/Pd/PMMA	11–14	25	–	25	2	N_2	420	0.06	5	0.37	0.4	[41]
								Air		0.6	>2	0.38	0.7	
	Strain eng. Pd MOTIFE	Pd	10	100	100	25	2	Air	103	0.2		<1	<1	[44]
				100	400				101	0.1		<1	<1	[44]
				100	800				92	0.05		<1	<1	[44]
				30	800				357	0.8		–	–	[45]
				60	800				254	0.2		–	–	[45]
				90	800				104	0.05		–	–	[45]
				120	800				94	0.005		–	–	[45]
	Pd MOTIFE linked TFT	Pd+InGaZnO TFT	10	25	–	25	4	N_2	50	0.04		1–2	1–2	[40]
	Thermal stability test	Pd	10	50	–	25	10	N_2	–	0.3	>2	<1	–	[47]
						80			–	0.5				
						90			169	1				
						100			–	2				
						120			200	2				
						150			295	2				
						200			430	No signal				
CPE	CPE	Pd	<8	0	–	25	4	N_2	–	Off	–	–	–	[37]
			9, 10						–	0.5	2	–	–	
			11						900	0.4	2	<1	<1	
			>12						–	On	–	–	–	
	LNF-CPE	Pd	10	0	–	25	5	N_2	90	0.03	2	<1	–	[38]
	Patterned CPE	Pd	10	0	–	25	2	Air	<100	0.1	1.6	<1	<1	[42]
NRB	Stamped Pd NRB	Pd	30	0	–	25	12	Air	>100	2	>12	>100	<50	[43]
	Stamped PdAu NRB	0.6:0.4	15	0	–	25	10	Air	15	0.005	10	<100	<100	[48]
	Nanoimprinted Pd NRB	Pd	60	0	–	25	4	N_2	60	1.4	3.5	500	<200	[49]

**ADVANCED
SCIENCE NEWS**

www.advancedsciencenews.com

**ADVANCED
MATERIALS**

www.advmat.de

2. Fundamentals

2.1. H$_2$-Induced Lattice Expansion in Pd

H$_2$ can be absorbed by various materials to form metal hydrides,[50] nonmetal hydrides,[51] and complex hydrides.[52] Among these materials, transition metals (TMs) have attracted much attention for use as H$_2$ absorbents because of their high density of states (DOS) near the Fermi level and moderate electronegativity compared to H$_2$. However, the enthalpies of formation (ΔH) for binary metal hydrides are found to be positive, indicating inefficient H$_2$ absorption, for most transition metals in group 6 to 11 except for Pd, Ni, and Cr.[53] Among these three metals for which ΔH is negative, only Pd forms a stable hydride;[54] Pd also possesses the lowest activation energy for H$_2$ diffusion from the surface to the subsurface layer, which is advantageous for H$_2$-sensing.[55] The absorption of H$_2$ by Pd induces an expansion of the metal lattice. Pd has a fcc structure with a lattice constant of a = 0.3890 nm.[56] Two kinds of interstitial sites exist in fcc Pd: one octahedral and two tetrahedral sites per Pd atom.[57] Despite the theoretical calculations that tetrahedral sites are energetically more favorable than octahedral sites, disregarding the zero-point energy of H$_2$, H atoms tend to occupy the octahedral site in Pd because the sharper vibrational potential at the tetrahedral site causes a higher zero-point energy than at the octahedral site.[58]

The reaction steps between H$_2$ gas and Pd are presented in **Figure 7**a. When Pd is exposed to H$_2$ gas, the H$_2$ molecules physisorb on the Pd surface by the van der Waals force. Then, H$_2$ molecules dissociate into H atoms on the Pd surface and subsequently diffuse into Pd. These chemisorbed H atoms occupy the octahedral sites of the fcc Pd lattice. This reaction occurs spontaneously at room temperature and atmospheric pressure.

The occupation of interstitial sites by H$_2$ results in lattice expansion in Pd due to lattice distortion, forming Pd hydride. In the Pd–H system, Pd hydride can exist in two different phases, α and β phases. Contrary to what one can infer from its name, Pd hydride is an alloy of Pd with metallic H$_2$, which is different from ionic hydride. Upon H$_2$ absorption at low H$_2$ pressure, H atoms are slightly dissolved into Pd, causing partial filling of interstitial sites to form the α phase, a solid-solution phase (Figure 7b). With increasing H$_2$ pressure, the amount of absorbed H$_2$ increases and reaches the maximum boundary of α phase $n_{\alpha max}$ = 0.02 (n = H/Pd, atomic ratio of absorbed H relative to Pd) at room temperature.[59] At this boundary, a first-order transition occurs in the PdH matrix, where the nuclei of the β phase start to form in the α phase with the large uptake of H$_2$, and subsequently the α and β phases coexist until the minimum boundary of the β phase $n_{\beta min}$ = 0.58 at room temperature.[59] The region between $n_{\alpha max}$ and $n_{\beta min}$ is called the miscibility gap, which becomes narrower as the temperature increases. The absorption of H$_2$ in this region occurs at a nearly constant pressure, which is called the plateau pressure. This plateau pressure arises from the reordering of the α to β transition. Above the ratio of n = 0.58, the α phase completely disappears, and only the β phase exists in the system at room temperature.

The lattice constant of the α phase expands with increasing H absorption, and when n = 0.02, it reaches a maximum $a_{\alpha, max}$ of 0.3895 nm, which is 1.3% longer than that of pure Pd at room temperature (Figure 7c).[57] The formation of the β phase with increased H$_2$ solubility accompanies the large H$_2$ absorption, which induces a larger lattice expansion than that of the α phase. The minimum lattice constant of the β phase is $a_{\beta, min}$ = 0.4025 nm, and it increases to a_β = 0.4040 nm (at n = 0.7) with a higher H$_2$ pressure in the Pd hydride at room temperature.[57]

2.2. H$_2$ Sensing Mechanism of Pd Nanogaps

The MOTIFEs and CPEs detect dilute H$_2$ with numerous Pd nanogap arrays formed on an elastomeric substrate. These sensors can be fabricated through simple and continuous processes without conventional complicated processes such as lithography because the nanogaps are spontaneously induced by the elasticity of the substrate. **Figure 8**a shows the sequence of processes required to fabricate a typical MOTIFE. As the elastomeric substrate, PDMS has remarkable mechanical elasticity with chemical inertness to H$_2$ and without interdiffusion with Pd.[18] First, a Pd thin film was deposited on the PDMS using the sputtering process (Figure 8b), and then the entire sample was elongated in a direction (x) using a stretching machine with controlled strain (Figure 8c). In the sputtering process, the surface of PDMS is exposed to Ar plasma and converted into silica.[60,61] As a result, cracks are generated on the hardened surface during the subsequent stretching process, and the Pd film is broken at these positions. The broken films separated by cracks are slightly elongated compared to the initial state along the stretching direction because they undergo tensile strain until just before breaking. Therefore, when the PDMS substrate returns to its original state after the tensile strain is removed, the cracks are closed by the overlap of the broken Pd films (Figure 8d). At this time, the Pd films build a closed circuit through which current can flow. The nanogaps were formed after the edges of the broken Pd films were crushed and deformed during the expansion of the Pd films due to the initial exposure to H$_2$, and the system finally becomes an open circuit (Figure 8e). This nanogap formation mechanism based on Pd expansion and deformation has been quantitatively verified by a systematic study on the nanogap width with respect to the H$_2$ concentration of the initial exposure, as described in detail in Section 3.3.[39]

On the other hand, in the fabrication procedure of typical CPE, a mechanical stretching process for inducing cracks on the Pd film was not required. As shown in Figure 8f, the nanogaps of CPE are only generated by conducting the initial H$_2$ exposure process for the Pd film deposited on PDMS. The expansion of the Pd film due to the absorption of H$_2$ induces a tensile strain on the PDMS substrate.[37] As a result, the Pd film is deformed owing to the relative compressive stress during the transformation into β Pd hydride and volume expansion. Finally, when H$_2$ is removed, the Pd film is cracked owing to the tensile strain caused by the deformation, forming the nanogaps. Therefore, in CPE, the nanogap is formed randomly, and the width of the nanogaps (900 nm) is larger than that of the Pd MOTIFE (300 nm) because the nanogap originates from the shrinkage of the entire Pd film rather than the deformation at the edge of the broken Pd films.[37]
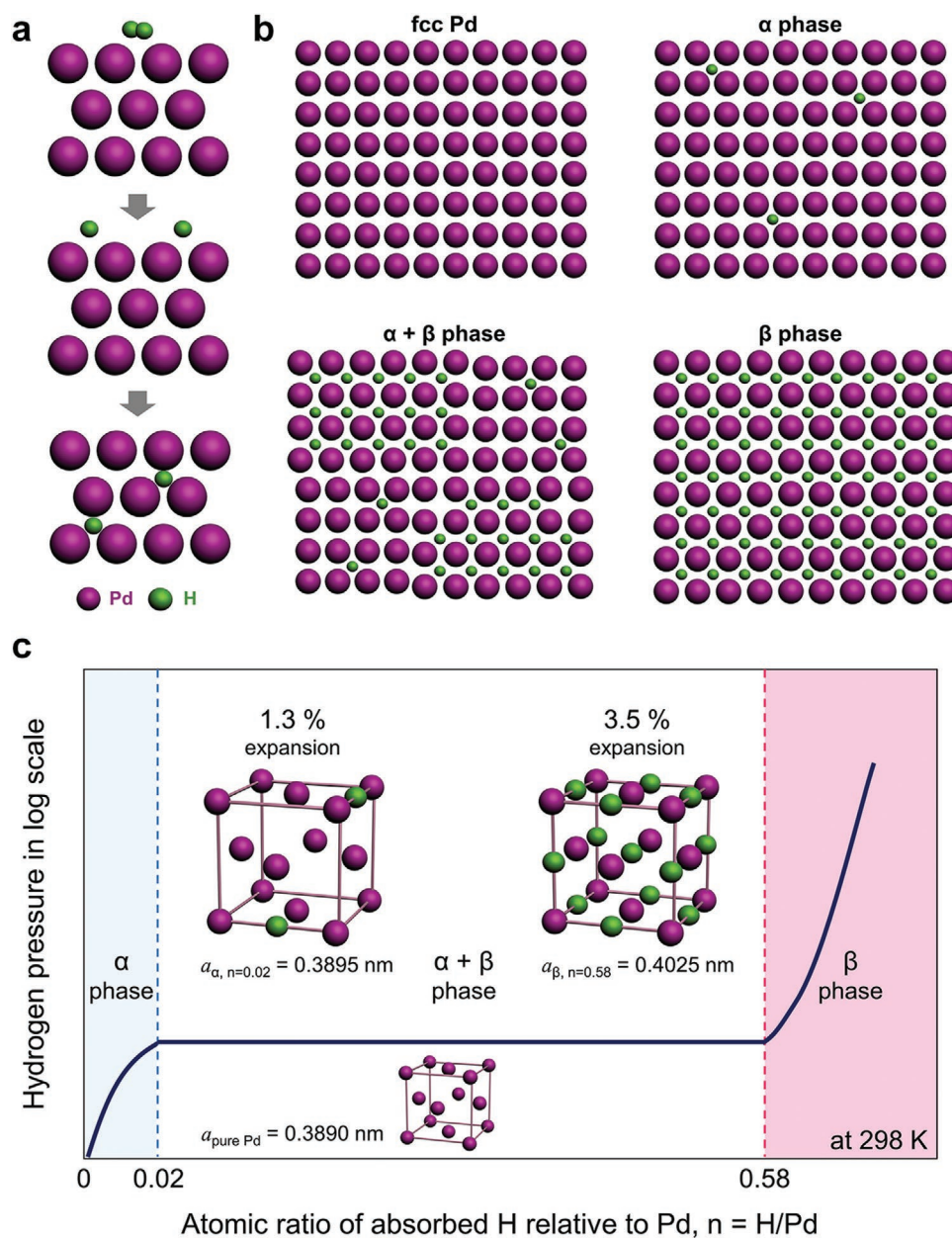
**ADVANCED
SCIENCE NEWS**

www.advancedsciencenews.com

**ADVANCED
MATERIALS**

www.advmat.de

Figure 7. Pd–H reaction. a) Reaction steps between H_2 molecule and Pd. b) Schematic illustrations for (100) surfaces of fcc Pd and the phases formed during H_2 absorption. c) A schematic of pressure–composition–temperature (PCT) curve of Pd–H absorption processes with several lattice shapes of Pd–H system at room temperature.

The PDMS substrates used in the Pd MOTIFEs and CPEs were prepared with a thickness of 0.75 mm using a 10:1 weight ratio of the base resin and curing agent mixture, followed by curing at 70 °C for 3 h. Pd thin films with a thickness of ≈10 nm were deposited using Ar plasma sputtering at a base pressure of ultrahigh vacuum. In the case of Pd MOTIFEs, the samples were elongated by 25% of the tensile strain, which is defined as $\varepsilon = [(L - L_0)/L_0] \times 100\%$, where L and L_0 are the stretched and initial lengths of the sample, respectively. The initial H_2 concentration was 4% for both cases.[18,37]

Figure 9a shows the real-time electrical response of a Pd MOTIFE obtained at various H_2 concentrations, in which

a clear on–off sensing operation was observed. The Pd films of MOTIFEs are in an electrically disconnected "off" state due to the nanogaps formed by the initial H_2 exposure. As the H_2 concentration increased, the width of the nanogaps decreased owing to the Pd expansion. When an electrical path is formed on the entire Pd films by closing some of the nanogaps above a certain H_2 concentration, a minute current begins to flow in the "on" state, and an electrical sensing signal can be observed. As the H_2 concentration further increased, the number of closed nanogaps increased and numerous electrical paths were formed on the Pd films. As a result, the resistance of the entire Pd film decreased, resulting in a larger current signal. The
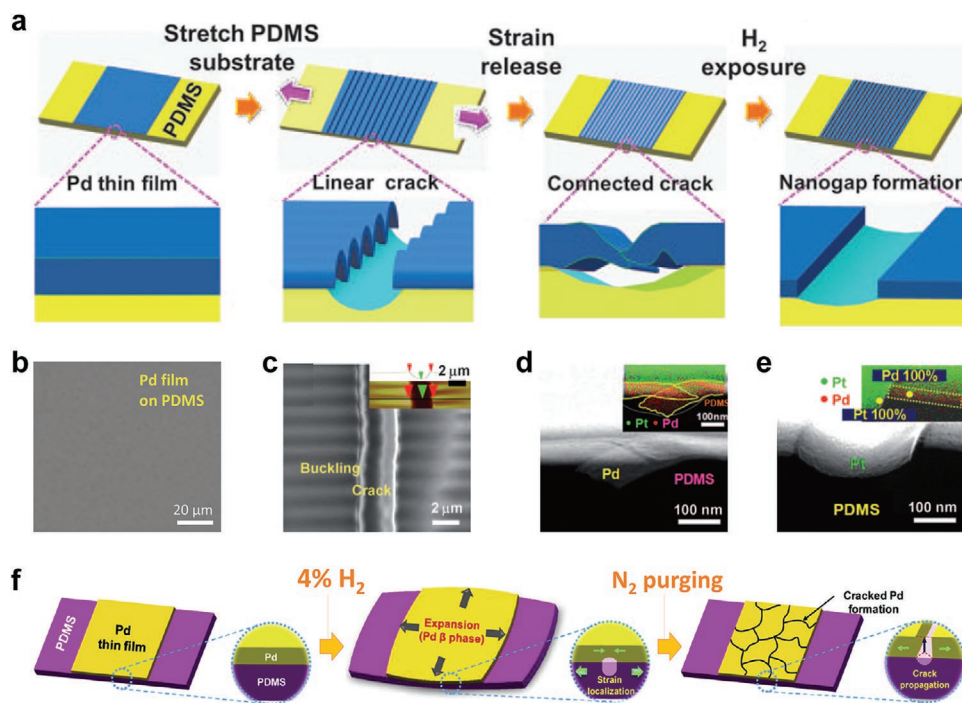
Figure 8. a) Schematic diagrams of Pd nanogap formation procedure on an elastomeric substrate for the fabrication of Pd MOTIFE. From the left, a Pd film deposited on a PDMS substrate, PDMS cracks and broken Pd films induced by the mechanical stretching process, the broken Pd films overlapped each other by the strain removal, and Pd nanogaps formed by the initial H_2 exposure process are represented, respectively. b–e) Scanning electron microscope (SEM) images for the Pd film, crack, overlapped Pd films, and Pd nanogap. The inset in (c) is an atomic force microscope (AFM) image of the crack. The insets in (d) and (e) show the elemental mapping of the overlapped Pd films and Pd nanogap, respectively, which are obtained from the cross-sectional transmission electron microscopy (TEM) technique. Reproduced with permission.[18] Copyright 2011, Wiley-VCH GmbH. f) Schematics of Pd nanogap formation process for fabrication of CPE. From left, the deposition of Pd film, the initial H_2 exposure, and nanogap formation during H_2 removal. Reproduced with permission.[37] Copyright 2012, Elsevier B.V.

Pd MOTIFE with the nanogaps, formed by the initial exposure to 4% H_2, showed the first electrical response at a H_2 concentration of 0.05%. However, the detection limit was found to be 0.4% after exposure to a high concentration of 10% H_2 because the Pd films undergo an additional edge deformation owing to the maximum expansion.[18] Another main feature of the Pd nanogap-based H_2 sensors is the discernibility at high H_2 concentrations. As shown in Figure 9a, the Pd MOTIFE shows a linear response depending on the H_2 concentration less than 2%, but the current is saturated at higher than 2% H_2. This is due to completion of the α to β phase transition by sufficient H_2 concentration and will be discussed in detail in Section 5.2.

The on–off sensing mechanism based on the Pd nanogaps was quantitatively revealed in an intensive study on the sensing mode of CPEs depending on the thickness of the deposited Pd film.[37] As shown in Figure 9b, the electrical responses were obtained through repeated H_2 exposure and removal based on Pd thin films of varying thickness from 6 to 14 nm. When the thickness of the Pd film of CPE was greater than 11 nm, cracks on the PDMS were induced by the Pd expansion during the initial H_2 exposure, but the thickness of the Pd film was too thick for the cracks to completely cut the film and to form nanogaps. As a result, the CPE operated as an on-mode sensor that could not obtain the complete off state without current flow. On the other hand, in a CPE with a thickness of less than 9 nm, the cracks and nanogaps were easily formed by the

initial H_2 exposure, but the expandability of the Pd films upon repeated H_2 exposure was not sufficient to overcome the support of the PDMS substrate and close the nanogap. Therefore, as the test was repeated, the sensor settled in off mode where no further electrical response was observed. Definite on–off sensing mode could be observed in the CPEs with a thickness range of 9–11 nm, and the MOTIFEs and CPEs to be introduced later were fabricated based on Pd films with a thickness of ≈10 nm.[36–42,44–46]

3. Strategies for Controlling Width of Nanogaps

3.1. Ni Alloying

After on–off sensing signals of at least 0.4% H_2 concentration were first demonstrated using a pure Pd-based MOTIFE, Ni alloying was immediately attempted to effectively reduce the detection limit of MOTIFEs.[18] In terms of mechanical characteristics, Ni has higher ductility and fracture toughness compared to Pd.[62] Therefore, a small amount of Ni added to the Pd film increases the ductility and toughness of the film,[63] and the film is further elongated prior to crack formation in the initial stretching, which is the first step in the formation of nanogaps. As a result, the width of the finally formed nanogap was decreased; in the $Pd_{87.5}Ni_{12.5}$ MOTIFE,
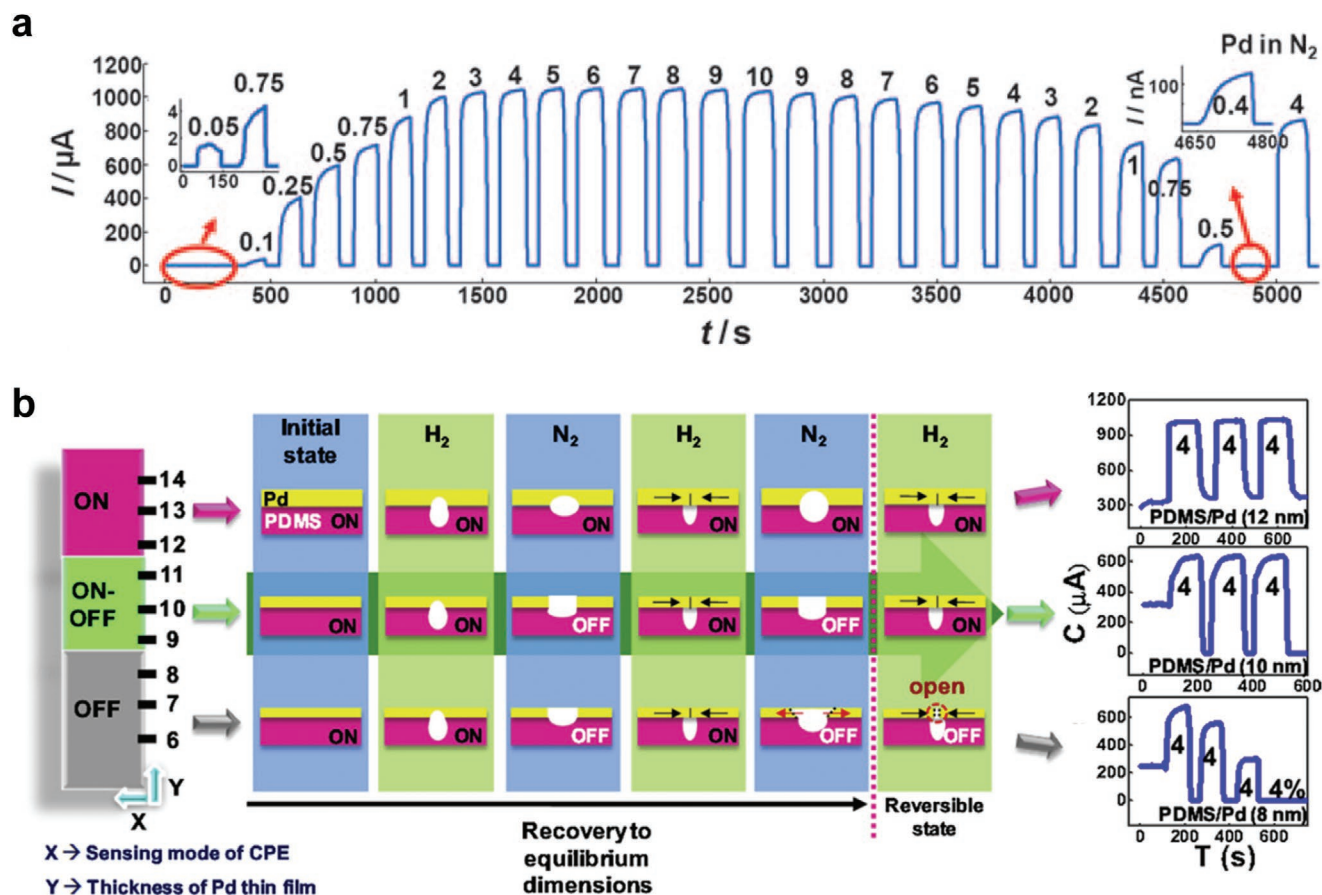
Figure 9. a) The real-time electrical response of a Pd MOTIFE to various H_2 concentrations based on N_2 carrier at room temperature. The numbers on top of the electrical response indicate the H_2 concentration in percentages, and the detection limit was found to be 0.4%. Reproduced with permission.[18] Copyright 2011, Wiley-VCH GmbH. b) Schematic diagram of the nanogap formation and sensing mode according to Pd thickness in CPEs. The real-time electrical responses presented on the right side indicate that the CPEs with Pd thickness of 12, 10, and 8 nm operate in the on mode, on–off mode, and off mode, respectively. Reproduced with permission.[37] Copyright 2012, Elsevier B.V.

the average nanogap width (62 nm) was approximately one-third of the nanogap width of the pure Pd MOTIFE (218 nm), as shown in **Figure 10**a,b.[36] The decrease in the nanogap width causes a reduction in the detection limit by allowing the nanogap to close despite slight film expansion due to a lower amount of H_2 exposure.

Furthermore, Ni alloying affects the expandability of the film due to H_2 exposure as well as mechanical properties. Figure 10c shows the relative volume change ($\Delta V/\Omega$) of the PdNi alloy due to H_2 absorption as a function of Ni content, where ΔV and Ω are the volume change and initial volume, respectively. Ni alloying increases the relative volume change caused by a decrease in the lattice constant and thus, reduces the detection limit by increasing the film expansion at the same H_2 concentration.[36,64] It is noted that a Ni content of ≈20% would rather increase the detection limit because of the decrease in H_2 solubility.[65]

Consequently, Ni alloying effectively reduces the detection limit of the MOTIFE through synergies of two different effects: reducing the nanogap width and increasing the expandability of the Pd film. A detection limit of ≈0.1% obtained from $Pd_{93}Ni_7$ alloy-based MOTIFE was reported along with the pure Pd MOTIFE,[18] and a 100 ppm detection limit was achieved for

the optimized PdNi alloy MOTIFE ($Pd_{87.5}Ni_{12.5}$) (Figure 10d),[36] which are 5-fold and 40-fold reductions compared to the pure Pd MOTIFE (0.4%), respectively.

In this PdNi alloy-based MOTIFE, it was quantitatively revealed that the detection limit of the MOTIFE was related to the large gap width of the film, which provided motivations for the various strategies to reduce the detection limit based on the nanogap modulation, as described below.

3.2. Liquid N_2 Freezing

As the correlation between the detection limit and nanogap width was recognized in PdNi alloy-based MOTIFEs, the LNF process was developed as an alternative route for controlling the nanogap width based on pure Pd films.[38] The LNF process was applied to both MOTIFEs and CPEs based on pure Pd films. In the LNF-CPE without the stretching process for artificial crack formation, liquid N_2 droplets were dropped on Pd films deposited on PDMS substrates. In the case of LNF-Pd MOTIFEs, aligned cracks were first formed on Pd films with stretching (25% tensile strain), followed by the LNF process. Therefore, the LNF-CPE has a random nanogap
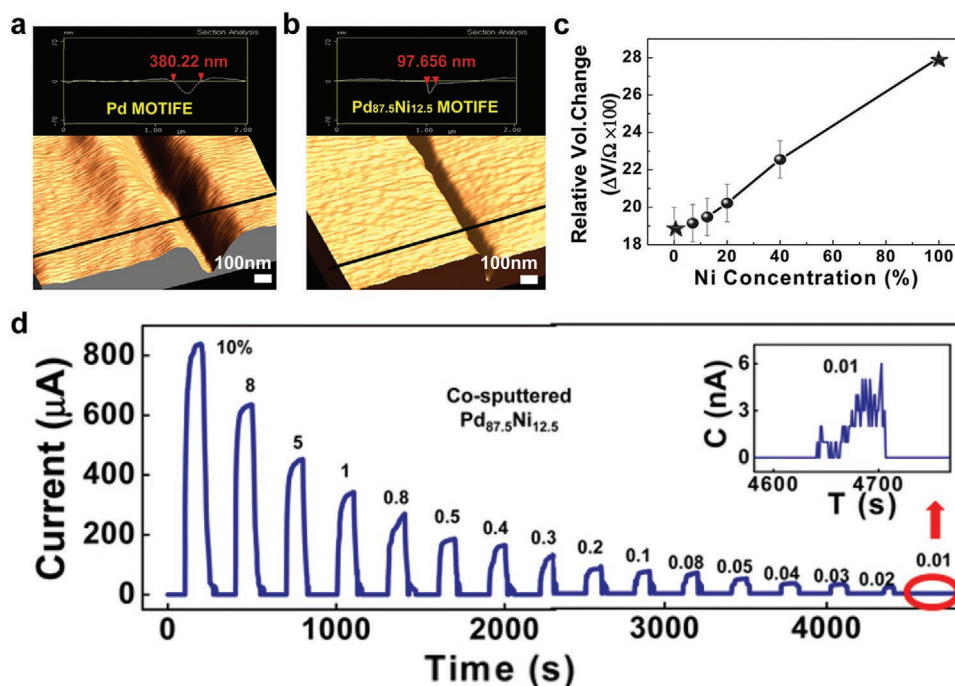
**ADVANCED
SCIENCE NEWS**

www.advancedsciencenews.com

**ADVANCED
MATERIALS**

www.advmat.de

Figure 10. AFM height profiles and images of nanogaps on a) a pure Pd and b) a $Pd_{87.5}Ni_{12.5}$ alloy MOTIFE. The nanogap width on a) the pure Pd MOTIFE is 380 nm and the nanogap width on b) the $Pd_{87.5}Ni_{12.5}$ alloy MOTIFE is 98 nm. The average nanogap width was found to be 218 and 61.8 nm for the pure Pd and $Pd_{87.5}Ni_{12.5}$ alloy, respectively. c) The relative volume change ($\Delta V/\Omega$) of PdNi alloy due to H_2 absorption as a function of Ni concentration. The values of pure Pd and Ni were obtained from ref. [64] and those of PdNi alloy were calculated in ref. [36]. d) The real-time electrical response of a $Pd_{87.5}Ni_{12.5}$ alloy MOTIFE to various H_2 concentrations in N_2 carrier at room temperature. The detection limit of the $Pd_{87.5}Ni_{12.5}$ alloy MOTIFE was found to be 100 ppm. Reproduced with permission.[36] Copyright 2012, Elsevier B.V.

in nature like a typical CPE,[37] while the LNF-Pd MOTIFE shows nanogaps aligned vertically with the stretching direction (**Figure 11**a,d).

In a typical CPE, cracks and nanogaps on a Pd film are formed via expansion and contraction of the Pd film by initial H_2 exposure, and in a typical Pd MOTIFE, nanogaps are formed at closed cracks after the initial H_2 exposure. In the case of the LNF process, however, the difference in the coefficient of thermal expansion (CTE) between the Pd film and the PDMS substrate acts as an additional driving force for the formation of cracks and nanogaps, while the strain in the Pd film is caused only by the initial H_2 exposure in the typical process.[38] Because the CTE of PDMS is larger than that of Pd, the LNF process applies tensile and compressive strains to the PDMS substrate and Pd film, respectively.[66–68] The subsequent recovery process occurs more rapidly on the PDMS substrate compared to the Pd film, which generates cracks in LNF-CPEs and affects the formation of nanogaps in both LNF-CPEs and LNF-Pd MOTIFEs. In the LNF process, the cracks on the PDMS substrate contract, resulting in a smaller width of nanogaps than the typical process without LNF after the initial H_2 exposure.[38] In the case of LNF-Pd MOTIFEs, the compressive strain originating from thermal contraction can be released through the aligned cracks and overlapping of broken Pd films, leading to a smaller nanogap width compared to that of LNF-CPE. The average nanogap width of LNF-CPE was estimated to be 80–120 nm, as shown in Figure 11b.[38] These values are close to one-tenth that of typical CPE (900 nm).[37] In the case of LNF-Pd MOTIFEs, it was found to be ≈25 nm (Figure 11e),[38]

which was much smaller than the LNF-CPE case and approximately tenfold smaller than that of typical Pd MOTIFEs (200–300 nm).[18,36]

In the real-time H_2 sensing test, it was demonstrated that the decrease in the nanogap width caused by the LNF process effectively reduced the detection limit of both LNF-CPEs (300 ppm) and LNF-Pd MOTIFEs (200 ppm),[38] which are less than one-tenth of the detection limit of typical CPEs (0.4%) and Pd MOTIFEs (0.4%).[18,37] These values are slightly higher than those of the optimal PdNi alloy MOTIFE (100 ppm), and even in the case of LNF-Pd MOTIFEs, the nanogap width (25 nm) is smaller than that of the PdNi alloy (60 nm),[36] which can be attributed to the smaller H_2 expandability of pure Pd compared to that of the PdNi alloy.

3.3. Initial H_2 Concentration

As the H_2 sensing mechanism of MOTIFEs was revealed in detail, and the correlation between the nanogap width and detection limit was systematically investigated, a methodology to achieve an extremely low detection limit through control of the nanogap formation process based on the initial H_2 exposure was proposed.[39] As shown in **Figure 12**a, uniaxial stretching, the first step of the nanogap formation process, causes cracks on the PDMS substrate, and the plastically elongated and broken Pd films overlap with each other after the strain is released. The contact crack is finally converted into a nanogap through plastic deformation of the overlapped Pd films during
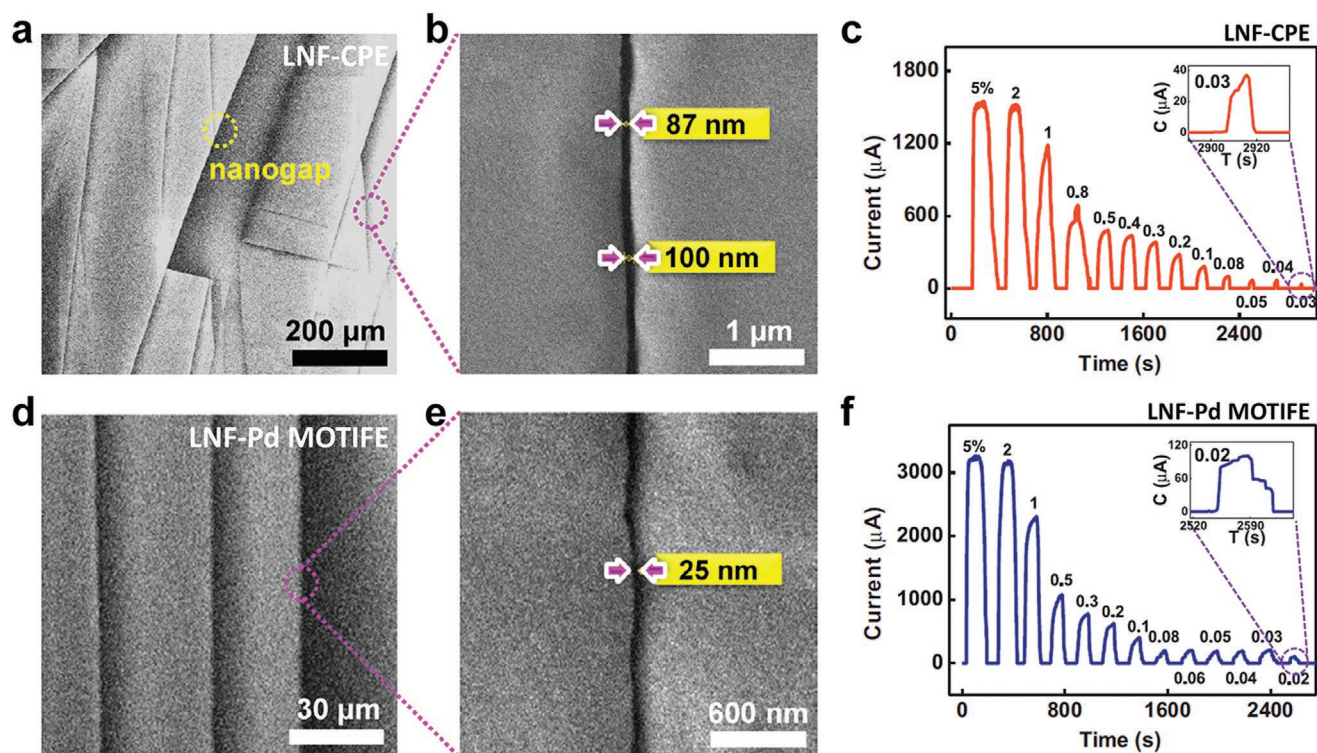
Figure 11. Low magnification SEM images of a) random nanogaps on an LNF-CPE and d) aligned nanogaps on an LNF-Pd MOTIFE. High magnification SEM images of a nanogap on b) the LNF-CPE and e) the LNF-Pd MOTIFE. The average nanogap width was estimated to be 80–120 nm and ≈25 nm for the LNF-CPE and the LNF-Pd MOTIFE, respectively. The real-time electrical response of c) an LNF-CPE and f) an LNF-Pd MOTIFE to various H_2 concentrations in N_2 carrier at room temperature. The detection limits of the LNF-CPE and the LNF-Pd MOTIFE were found to be 300 and 200 ppm, respectively. Reproduced with permission.[38] Copyright 2013, Elsevier B.V.

the initial H_2 exposure process. Consequently, it was possible to reduce the nanogap width by minimizing the deformation of the overlapped Pd films by controlling the H_2 concentration of the initial exposure.[39]

Figure 12b,c shows cross-sectional transmission electron microscopy (TEM) images of a nanogap on Pd MOTIFEs after the initial exposure with 0.1% and 1.5% H_2 concentrations, respectively. Under a low concentration of H_2 exposure, the Pd film retains the α phase in which H_2 penetrates into the interstitial sites of the Pd matrix, and the maximum expansion is 0.13% of the lattice parameter.[69] On the other hand, at high H_2 concentrations, the α-phase Pd transformed into β Pd hydride, and this phase transition increased the lattice expansion to 3.47%.[70,71] As a result, the initial exposure to low H_2 concentration (0.1%) formed fine nanogaps with an overlapping structure, but the high concentration (1.5%) resulted in clear nanogaps caused by deformation of the broken Pd films. In this work, various initial concentrations from 0.1% to 5% were systematically tested, and the average nanogap width was found to be ≈8, 10, 40, and 53 nm for initial H_2 concentrations of 0.1%, 1.3%, 1.5%, and 2%, respectively.[39]

Figure 12d shows the detection limits obtained from the initial exposure controlled Pd MOTIFEs according to the H_2 concentration. At an initial exposure of less than 1%, the increase in the detection limit with increasing H_2 concentration was very small because the Pd film maintained the α phase. However, as the H_2 concentration increased above

1%, the detection limit increased significantly due to the α to β phase transition, and it can be seen that the phase transition was completed above 2%. The minimum detection limit obtained in the initial exposure controlled Pd MOTIFE was 10 ppm (0.1% initial H_2 concentration), which is the smallest value reported in MOTIFEs and a 400-fold reduction compared to the first Pd MOTIFE with a detection limit of 0.4% (10% initial H_2 concentration).[18] The detection limits of Pd MOTIFEs exposed to 1.5% and 3% H_2 were found to be 0.2% and 0.35%, respectively.[39] However, since the reproducibility of this α-phase Pd MOTIFE significantly decreases when exposed to a high H_2 concentration due to the phase transition, it can only be used in limited environments requiring extreme sensitivity as a one-time H_2 sensor.

3.4. Strain Engineering

The strategies introduced above for reducing the detection limit were mainly to control the nanogap width using post-treatment in the nanogap formation process after generating cracks. Here, an advanced route was attempted to reduce the detection limit by controlling the final nanogap width and density based on strain engineering in the crack generation procedure.[44,45] In these strain-engineered Pd MOTIFEs, mechanical stretching and compression repeated more than 20 times formed nanogaps on the Pd film as well
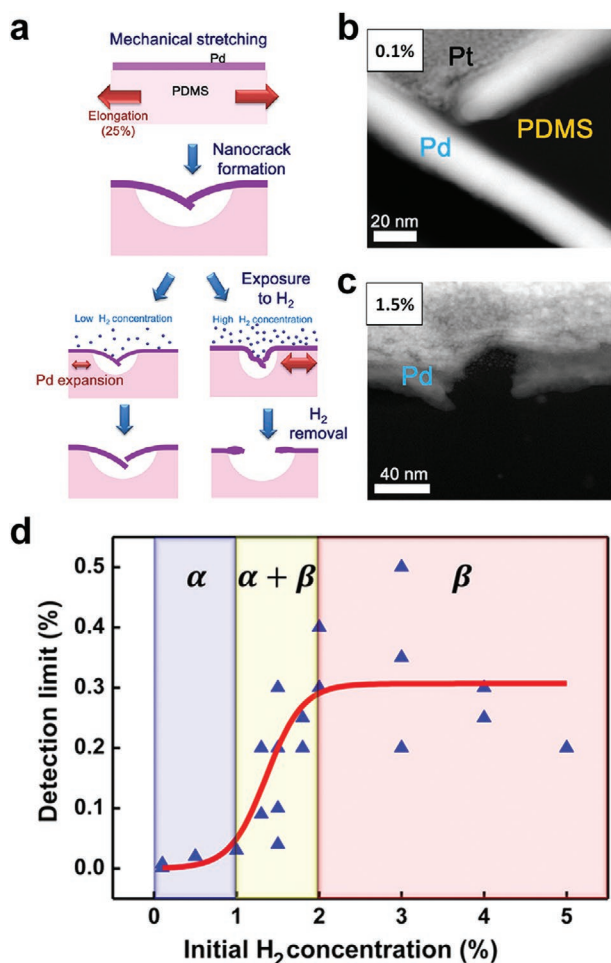
2005929 (12 of 26)

**ADVANCED
SCIENCE NEWS**

www.advancedsciencenews.com

**ADVANCED
MATERIALS**

www.advmat.de

Figure 12. a) Schematics of nanogap formation process for the nanogap width control based on the H_2 concentration of initial exposure. Cross-sectional TEM images of a nanogap on Pd MOTIFEs exposed to different initial H_2 concentration of b) 0.1% and c) 1.5%. The average nanogap width was found to be ≈8 and 40 nm for the initial H_2 concentration of 0.1% and 1.5%, respectively. d) The detection limits of the initial exposure controlled Pd MOTIFEs as a function of H_2 concentrations based on N_2 carrier at room temperature. Reproduced with permission.[39] Copyright 2013, Elsevier B.V.

as the cracks, and the measurement of the real-time electrical response to H_2 was conducted in air to determine the practical sensing performance.

First, the nanogap formation and detection limit of the strain-engineered Pd MOTIFEs were studied with variation in tensile velocity using a microtensile tester.[44] The strain magnitude was fixed at 100% of the original length. **Figure 13**a–c shows the configuration of nanogaps on Pd films generated at strain velocities of 100, 400, and 800 $\mu m\ s^{-1}$, respectively. A distinct feature of the strain-engineered Pd MOTIFEs was the horizontal nanogaps caused by buckling under tensile strain and cracking under compressive strain along the x-axis, while the vertical nanogaps were directly formed by the tensile strain.[44] The most noticeable impact of varying the tensile velocity was on the density of the nanogap. The nanogap density clearly increased to 380, 540, and 600 mm^{-1} for the vertical nanogaps and to 470, 630, and 670 mm^{-1} for the horizontal nanogaps, as

the tensile velocity increased. It was found that the increase in the nanogap density was due to the strain hardening effect, resulting in an increase in stress at the same strain.[44] On the other hand, the average nanogap width with increasing tensile velocity was 103, 101, and 92 nm for the vertical nanogaps and as 63, 56, and 54 nm for the horizontal nanogaps, which are insignificant compared to the variation in density. Therefore, the reduction in detection limit of 0.2%, 0.1%, and 500 ppm as the tensile velocity increased to 100, 400, and 800 $\mu m\ s^{-1}$, respectively, could be attributed to the increase in the nanogap density that accompanies H_2 permeation.[44]

Next, the nanogap formation and detection limit of the strain-engineered Pd MOTIFEs were investigated by focusing on the strain magnitude.[45] In this work, the tensile strain in the repeated mechanical stretching and compression was varied from 30% to 120% with a fixed strain of 800 $\mu m\ s^{-1}$. It was noted that the Pd MOTIFEs fractured at tensile strains above 130%.[45] Figure 13d–g shows the configuration of nanogaps generated by strains of 30%, 60%, 90%, and 120%, respectively. As depicted in the inset, the nanogap density increased with increasing strain. The average nanogap density was found to be ≈450, 550, 1350, and 1470 mm^{-1} for strains of 30%, 60%, 90%, and 120%, respectively. Horizontal nanogaps were observed in strains of 90% and 120%, indicating that the horizontal nanogaps were generated above a certain strain magnitude regardless of the tensile velocity.[44,45] Moreover, the increase in tensile strain resulted in an obvious reduction in the nanogap width compared to the case of tensile velocity. The average widths of the vertical nanogaps were estimated to be 357, 254, 104, and 94 nm for strains of 30%, 60%, 90%, and 120%, respectively.

The detection limits of 30%, 60%, 90%, and 120% strained Pd MOTIFEs were determined to be 0.8%, 0.2%, 500 ppm, and 50 ppm, respectively (Figure 13h). The significant reduction in the detection limit can be attributed to both the decrease in nanogap width and increase in nanogap density.[45] As shown in Figure 13i, in the strain range of 90% to 120%, a rapid reduction in the detection limit was observed despite the similar nanogap width, which can be explained by the increase in nanogap density. On the other hand, the correlation between the nanogap density and the detection limit obtained in the strain range of 30% to 90% was considerably weak compared to the correlation between the nanogap width and the detection limit (Figure 13j). Consequently, the nanogap density becomes an important factor affecting the detection limit when the nanogap width is as small as 100 nm or less. These results are in good agreement with the previous prediction that the sensing performance would be proportional to the surface to volume ratio at H_2 concentrations below 1%.[72] The optimal detection limit of 50 ppm obtained from the strain-engineered Pd MOTIFE is 240-fold and 8-fold smaller than that of the typical Pd MOTIFE and Pd–PDMS hybrid MOTIFE in air environments, respectively.[41]

3.5. Heat Treatment

Recently, a new approach to reduce the detection limit of H_2 in an air environment has been reported based on the heat shrinkage of elastomeric substrates.[48] This technique was designed based on the stamped Pd NRB array fabricated
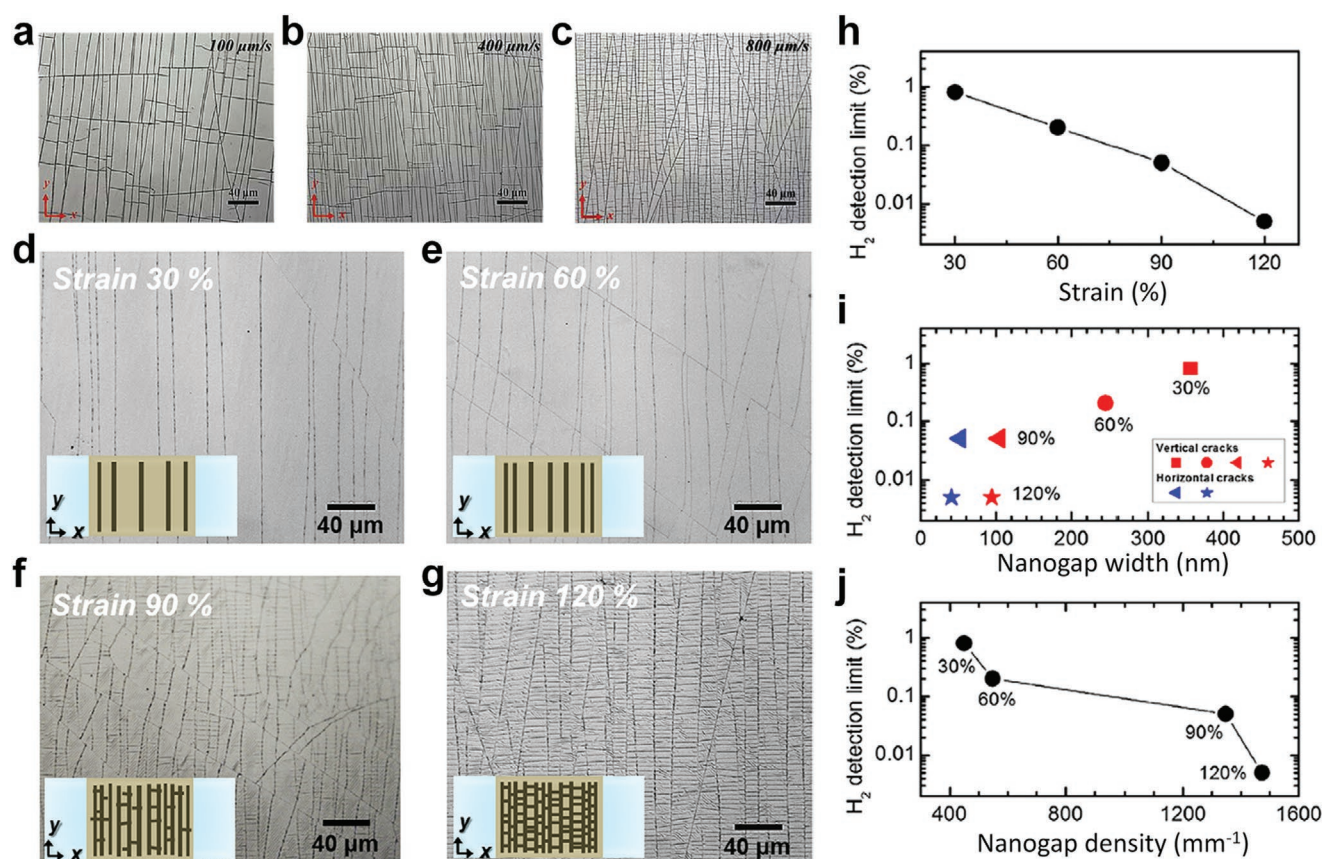
ADVANCED
SCIENCE NEWS
www.advancedsciencenews.com

ADVANCED
MATERIALS
www.advmat.de

Figure 13. Top-view OM images of nanogaps on the strain engineered Pd MOTIFEs generated by applying tensile stain of 100% with different tensile velocities of a) 100 μm s^{-1}, b) 400 μm s^{-1}, and c) 800 μm s^{-1}. Reproduced with permission.[44] Copyright 2016, Elsevier B.V. Top-view OM images of nanogaps on the strain engineered Pd MOTIFEs generated by applying different tensile strains of d) 30%, e) 60%, f) 90%, and g) 120% with the same tensile velocity of 800 μm s^{-1}. The insets indicate the schematic images of nanogaps on the strain engineered Pd MOTIFE. The H$_2$ detection limits in air obtained from the strain engineered Pd MOTIFEs as a function of h) the strain magnitude, i) the nanogap width, and j) the nanogap density. Reproduced with permission.[45] Copyright 2016, Springer Nature.

by the direct metal transfer (DMT) process using a nano-imprinted stamp, and the nanogap width was controlled by varying the temperature during the DMT process. The stamped NRB was first demonstrated using the pure Pd film and PET substrate (**Figure 14**a), and the H$_2$ detection limit was reported to be only 2% in air.[43] However, by controlling the heat treatment temperature in the DMT process based on the Pd$_{0.6}$Au$_{0.4}$ alloy thin film and PS substrate, 50 ppm of H$_2$ was detected, as shown in Figure 14b. Further, the minimum detection limit was estimated as 25 ppm based on the response curve obtained from a 15 nm nanogaps, which is the lowest value obtained for a Pd nanogap-based H$_2$ sensor in air.[48]

The DMT process was carried out at two different temperatures: the attachment temperature, at which the metal deposited stamp is placed on the substrate under pressure; and the detachment temperature, at which the metal film is transferred by removing the stamp. In this work, the detachment temperature was varied from 85 to 110 °C in 5 °C increments, the attachment temperature was fixed at 120 °C, and the width of the nanogap was investigated. As shown in Figure 14c, it was possible to reduce the nanogap width to 3 nm using this technique, which was attributed to the in-plane shrinkage of

the amorphous PS substrate.[48] Furthermore, in this stamped PdAu alloy NRB array, the β Pd hydride formation was sufficiently suppressed by Au alloying.

3.6. Detection Limit Based on Nanogap Width

Since a MOTIFE H$_2$ sensor based on the nanogaps of a Pd film was developed, the primary approach for reducing the low detection limit was to reduce the nanogap width, as mentioned above. **Figure 15**a is a schematic comparison showing the minimum nanogap width that has been demonstrated by various routes. The LNF process and the initial H$_2$ exposure control technique were applied to Pd MOTIFEs, and the reduction in the detection limit as the nanogap width decreased was successfully demonstrated (Figure 15b).[38,39] In the Ni alloying method, the reduction in nanogap width and detection limit was also confirmed.[36] Moreover, in CPEs with relatively large nanogap widths, a reduction in the nanogap width was observed using the LNF process; the detection limits lower than that of MOTIFEs at the same nanogap width were achieved because of the higher density of the randomly formed nanogap.[38] In the air-based tests focused on practical use, reduction in the
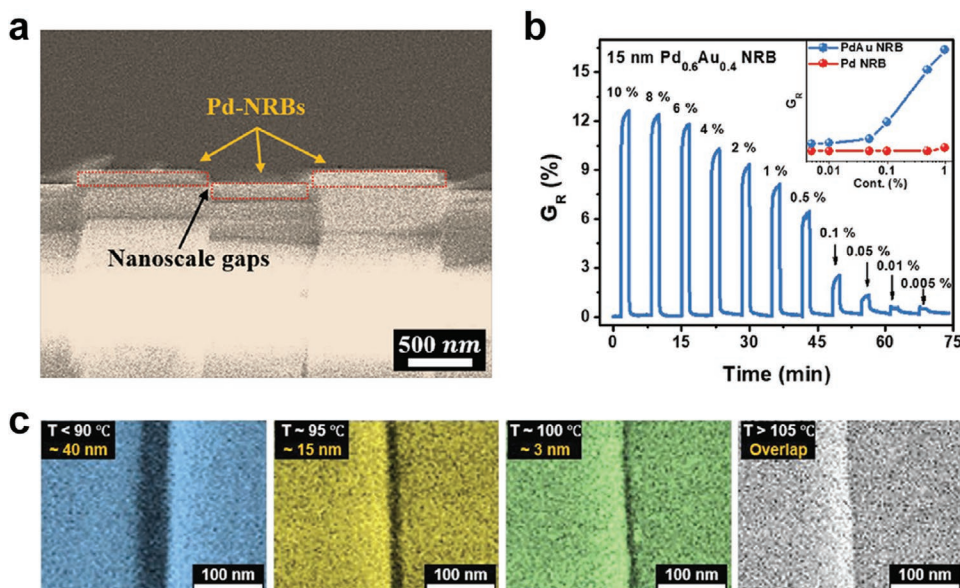
Figure 14. a) A cross-sectional SEM image of nanogaps in a stamped Pd NRB array on PET substrate fabricated by the imprint transfer technique. Reproduced with permission.[43] Copyright 2015, Wiley-VCH GmbH. b) The real-time electrical response of a stamped PdAu alloy NRB array on PS substrate to various H_2 concentrations in air at room temperature. The detection limit was found to be 50 ppm. c) Reduction of nanogap width of the stamped PdAu alloy NRB array using thermal shrinkage of the PS substrate during a heat treatment. Reproduced with permission.[48] Copyright 2019, Wiley-VCH GmbH.
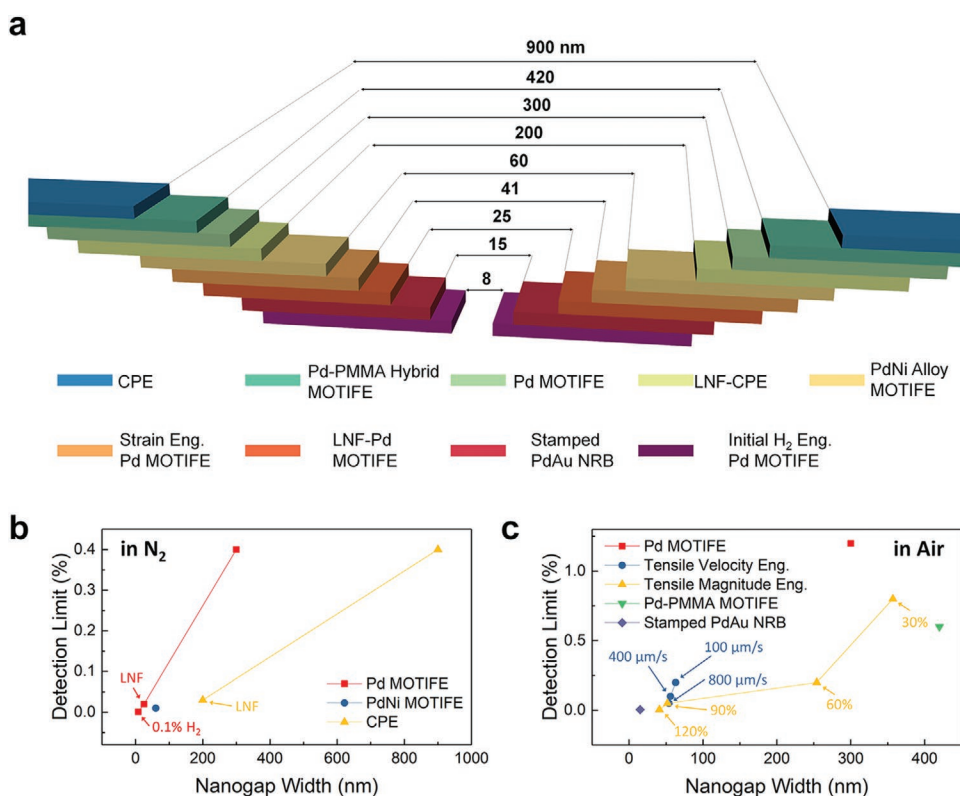
Figure 15. a) Schematic comparison of the minimum nanogap width in various MOTIFEs, CPEs, and stamped NRB. The H_2 detection limits of the various MOTIFEs, CPEs, and stamped NRB as a function of the nanogap width in b) N_2 and c) air environments. The nanogap width and detection limit data of Pd MOTIFE,[18] CPE,[37] PdNi alloy MOTIFE,[36] LNF-Pd MOTIFE,[38] LNF-CPE,[38] Pd MOTIFE with low H_2 exposure,[39] strain engineered Pd MOTIFE,[44,45] Pd–PMMA hybrid MOTIFE,[41] and stamped PdAu alloy NRB[48] were obtained from previous works.

ADVANCED
SCIENCE NEWS
www.advancedsciencenews.com

ADVANCED
MATERIALS
www.advmat.de

detection limit with decreasing nanogap width was confirmed, and it was found that the nanogap density as well as the width were critical factors affecting the detection limit in the studies on strain engineering effects (Figure 15c).[44,45]

3.7. Connecting to a Thin-Film Transistor

Finally, a study on the reduction of detection limit by coupling with an oxide TFT, a very different approach from the route based on the decrease in nanogap width, was reported.[40] In this method, a typical Pd MOTIFE was connected to an amorphous InGaZnO (a-IGZO) TFT to make the Pd nanogaps act as an additionally coupled capacitor to the oxide gate. **Figure 16**a shows the transfer curves (drain current vs gate voltage) obtained from the a-IGZO TFT and Pd MOTIFE-linked TFT in N_2 and 0.04% H_2. The charge capacitance of the Pd nanogap depends on the distance between the broken Pd films, and the total capacitance (C_{total}) of the Pd MOTIFE-linked TFT is determined by the relationship $C_{total} = 1/((1/C_{gap}) + (1/C_{oxide}))$,

where C_{gap} and C_{oxide} are the capacitance of the Pd nanogap and oxide gate, respectively.[40] As a result, the decrease in the nanogap width even at low concentrations of H_2 causes a shift in the threshold voltage by changing the capacitance of the total system. In other words, a lower H_2 concentration can be detected by sensitive monitoring of the change in the nanogap width without exposure to sufficient H_2 to close the nanogap. Using this Pd MOTIFE-linked TFT, H_2 concentrations less than 0.05% were detected, and the sensing mechanism could also be used to estimate the nanogap width.[40] However, when exposed to a H_2 concentration sufficient to close the nanogap, the linked Pd MOTIFE loses its capacitance and becomes a resistor in the circuit; hence, the threshold voltage of the total system reaches the intrinsic value of the a-IGZO TFT (Figure 16b). Therefore, this system should only be applied to dilute H_2.

4. Reliability and Stability for Commercial Applications

4.1. Reliability in Ambient Atmosphere

The sensing performance of the MOTIFE H_2 sensor based on the nanogaps of a Pd film in ambient atmosphere was further improved by applying a PMMA filter layer to eliminate interference from O_2 and H_2O in air while the Pd MOTIFE is sensing. PMMA is a polymeric material that has a much higher permeability for H_2 than other gases, such as O_2 and N_2.[41] When PMMA is incorporated into Pd–PMMA thin films, the hybrid sensors can have great potential in realizing sensors that can be used in air without an additional filter system.

For the fabrication of Pd–PMMA hybrid nanogap sensors, a Pd thin film is sandwiched between thin PMMA layers on a flexible PDMS substrate, and Pd nanogaps are formed throughout the multilayers by mechanical stretching and initial H_2 exposure, as shown in **Figure 17**a. It was clearly observed that the Pd–PMMA hybrid nanogap sensors operate well as an on–off sensor, as shown in Figure 17b. In particular, the lower detection limit of this hybrid nanogap sensor for H_2 sensing was found to be 6000 ppm in air (Figure 17b) and 600 ppm in N_2 (Figure 17c). This H_2 detection limit is significantly improved compared to 1.2% in air (Figure 17d) and 4000 ppm in N_2 for the pure Pd nanogap sensor, respectively.[18]

As described in Section 3, the detection limit of a Pd nanogap sensor is closely related to the initial exposure concentration of H_2.[39] Figure 17e shows the response tests for an initial H_2 concentration of 0.2% and reproducibility in air atmosphere. The Pd–PMMA hybrid nanogap sensors exhibited a very low H_2 detection limit of 400 ppm, which is more than an order of magnitude less than the value obtained with the initial 2% H_2 in air (Figure 17b). In particular, this effect is not reproducible in the pure Pd nanogap sensor once the sensor is exposed to H_2 gas at a concentration higher than that of the initial level. However, as shown in Figure 17e, the response signals for sweep-up (0.04–1% H_2) and sweep-down (1–0.06% H_2) were almost symmetric, and the low detection limit was similar to the first limit. The results indicate that in this hybrid Pd nanogap sensor, the degradation of the detection limit and reproducibility could be delayed. Accordingly, this study demonstrated
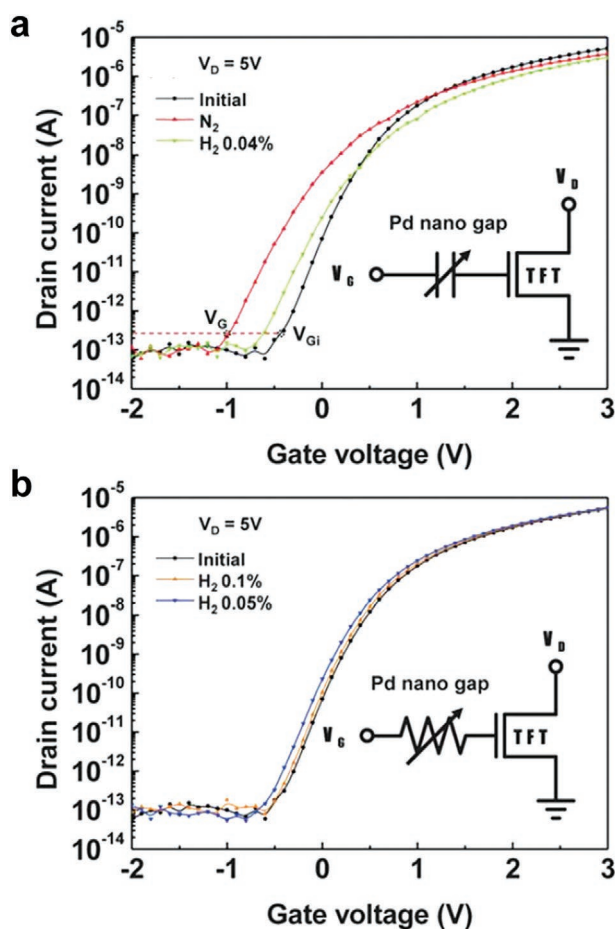

Figure 16. The transfer curves obtained from a Pd MOTIFE linked a-IGZO TFT with a) open and b) closed nanogap. The initial transfer curve shows the intrinsic property of the a-IGZO TFT without the Pd MOTIFE. The insets show the circuit configuration corresponding to each state of the Pd MOTIFE. Reproduced with permission.[40] Copyright 2013, Royal Society of Chemistry.
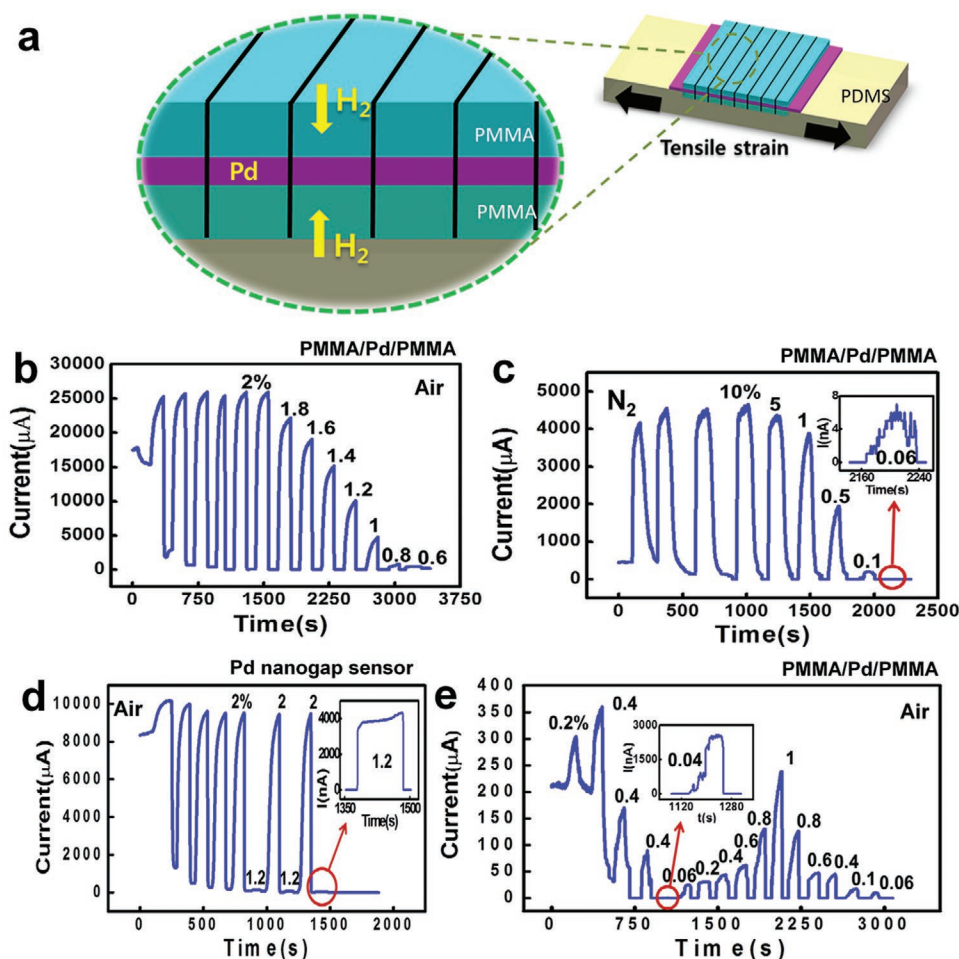
**ADVANCED
SCIENCE NEWS**

www.advancedsciencenews.com

**ADVANCED
MATERIALS**

www.advmat.de

Figure 17. a) Schematic diagram of the PMMA/Pd/PMMA hybrid nanogap sensor fabricated on a PDMS substrate. The real-time electrical responses at room temperature: a PMMA/Pd/PMMA hybrid nanogap sensor in b) air and c) N_2, d) a Pd nanogap sensor in air with initial H_2 concentration of 2%, and e) a PMMA/Pd/PMMA hybrid nanogap sensor in air with initial H_2 concentration of 0.2%. Reproduced with permission.[41] Copyright 2014, Elsevier B.V.

that the Pd–PMMA hybrid nanogap sensor has great promise in realizing sensors that can be utilized in ambient atmosphere without the use of additional filter systems.

Possible reasons for the reduced detection limit are selective H_2 permeation through the PMMA layers and the larger average distance between the nanogaps compared with that in the pure Pd film.[41] When a Pd film-based H_2 sensor is exposed to air, gaseous species, such as O_2, N_2, and H_2O, interact with the film surface and obstruct H_2 absorption onto the surface, reducing the ability to detect low H_2 concentrations.[73] Therefore, in the Pd–PMMA hybrid nanogap sensor, these interfering effects can be significantly reduced because of the top and bottom PMMA layers (**Figure 18**a). In addition, the maximum nanogap width that can be achieved by H_2 absorption is ≈1.07 μm for PMMA/Pd/PMMA trilayers with an average intercrack distance of 30.7 μm when assuming a 3.5% lattice expansion from α- to $\beta \cdot PdH_x$.[71] The average intercrack distance of the hybrid Pd film is approximately twice as large as that of a pure Pd film, as schematically shown in Figure 18b and measured in Figure 18c. Since the actual width of the nanogap was ≈420 nm, the detectable H_2 concentration could be further reduced.

In order to further improve the H_2-sensing performance of Pd nanogap-based sensors in ambient air, a new method to form narrow nanogaps without mechanical stretching was proposed.[42] **Figure 19**a presents the mechanism of nanogap formation. The Pd thin film was deposited on an elastomeric PDMS substrate patterned with a grating structure by NIL. To fabricate patterned PDMS, Si stamps with line patterns, which were fabricated by electron beam lithography, were used. The Pd nanogaps were formed on the edges of the PDMS grating by volume expansion/contraction of the Pd film after several cycles of H_2 absorption/desorption. Figure 19b shows the sensing mechanism of this nanogap sensor. When H_2 is absent from ambient air, electrons cannot transfer because of the nanogaps on the edge (OFF-mode). On the contrary, when H_2 is exposed, the nanogaps are closed due to lattice expansion through H_2 absorption, allowing electrons to transfer at the edge (ON-mode). The Pd nanogap formation on the edge of the Pd/PDMS grating was observed by TEM (scanning TEM (STEM)). The width of the Pd nanogap was ≈100 nm, which is smaller than that formed by mechanical stretching (≈300 nm) (top of Figure 19c).[18] The exact disconnection of

ADVANCED
SCIENCE NEWS
www.advancedsciencenews.com

ADVANCED
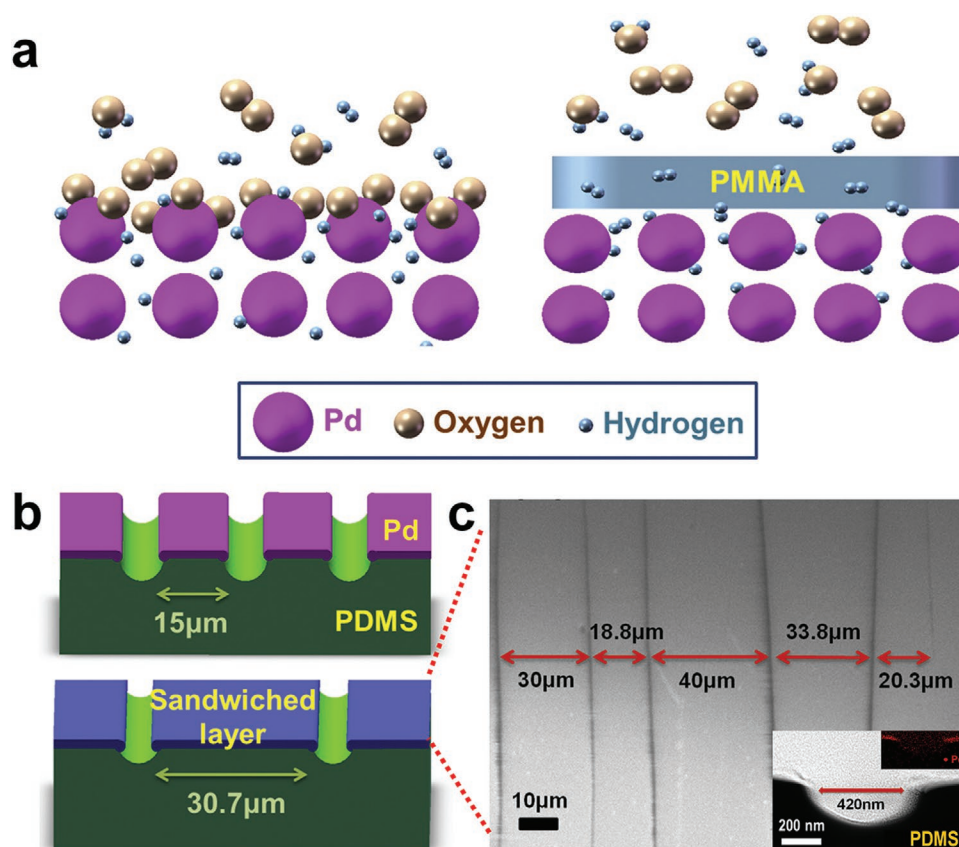MATERIALS
www.advmat.de

Figure 18. Schematic diagrams indicating the origins of the reduced H_2 detection limits of the PMMA/Pd/PMMA hybrid nanogap sensor. a) Left: Interaction of the Pd film with various gas species in an air environment; right: selective H_2 filtration through the PMMA layer and the consequent effective interaction between the Pd film and H_2. b) The difference between the average intercrack distances of the Pd nanogap sensor (top) and the PMMA/Pd/PMMA hybrid nanogap sensor (bottom). c) SEM image of the cracks formed in PMMA–Pd–PMMA/PDMS after the sample underwent mechanical stretching and consecutive cycle of exposure to air with and without H_2 (inset: a cross-sectional TEM image of portion of a crack and Pd EDX map). Reproduced with permission.[4] Copyright 2014, Elsevier B.V.

the Pd nanogap at the edge was confirmed by STEM elemental mapping images (bottom of Figure 19c).

Figure 19d shows the real-time current responses of the sensor for various H_2 concentrations at room temperature in air. The sensor exhibits perfect ON–OFF sensing behavior and a detection limit as low as 0.1% in air. The lower detection limit can be due to the small width of the nanogap. Figure 19e shows the repeatability tests of the sensor with H_2 concentrations of 0.2%, 0.7%, and 0.9% for 10 on/off cycles. It was observed that the current response was nearly constant without significant changes during repeated measurements. More repeatability tests (55 on/off cycles) were performed for 0.9%, which is the H_2 concentration that gave the best sensing performance, as shown in Figure 19f. The results showed good repeatability with consistent current response in each cycle. This indicates that this newly proposed Pd nanogap sensor maintained good reliability and rapid response time for a long period of ≈8000 s.

4.2. Stability in Humid Conditions

To evaluate the sensor's practical application in ambient atmosphere, the effect of humidity on the H_2-sensing performance of

Pd-based MOTIFEs was investigated. The Pd MOTIFEs were prepared with a tensile strain of 50% and an initial exposure of 0.5% H_2.[46] The average distance between adjacent nanogaps of the as-prepared sensors was ≈15 μm, which is the same as that typically formed on PDMS.[18] The Pd nanogap width of this sensor is ≈50 nm, which is six times smaller than those fabricated on Pd MOTIFEs prepared with an initial H_2 concentration of 10%.[18] **Figure 20**a shows the real-time current measurement results of the Pd-based MOTIFEs for different H_2 concentrations (0.04%, 0.06%, 0.08%, and 0.1%) at different relative humidity (RH) conditions ranging from 0% to 90% RH at room temperature. Figure 20b shows the saturated current values for different H_2 concentrations as a function of RH, which are shown in Figure 20a. As shown in Figure 20b, the saturated current values decreased slightly with increasing RH for all H_2 concentrations. This is attributed to the decreased number of active sites available for H_2 adsorption due to the increased adsorption of water molecules on the Pd film surface. This obstruction is more apparent at low H_2 concentrations. In general, it is known that elastomeric substrates are vulnerable to humidity. However, the results revealed that the sensing performance of the Pd-based MOTIFEs did not significantly degrade at H_2 concentrations of 0.1%, even under high RH conditions of 90% RH.
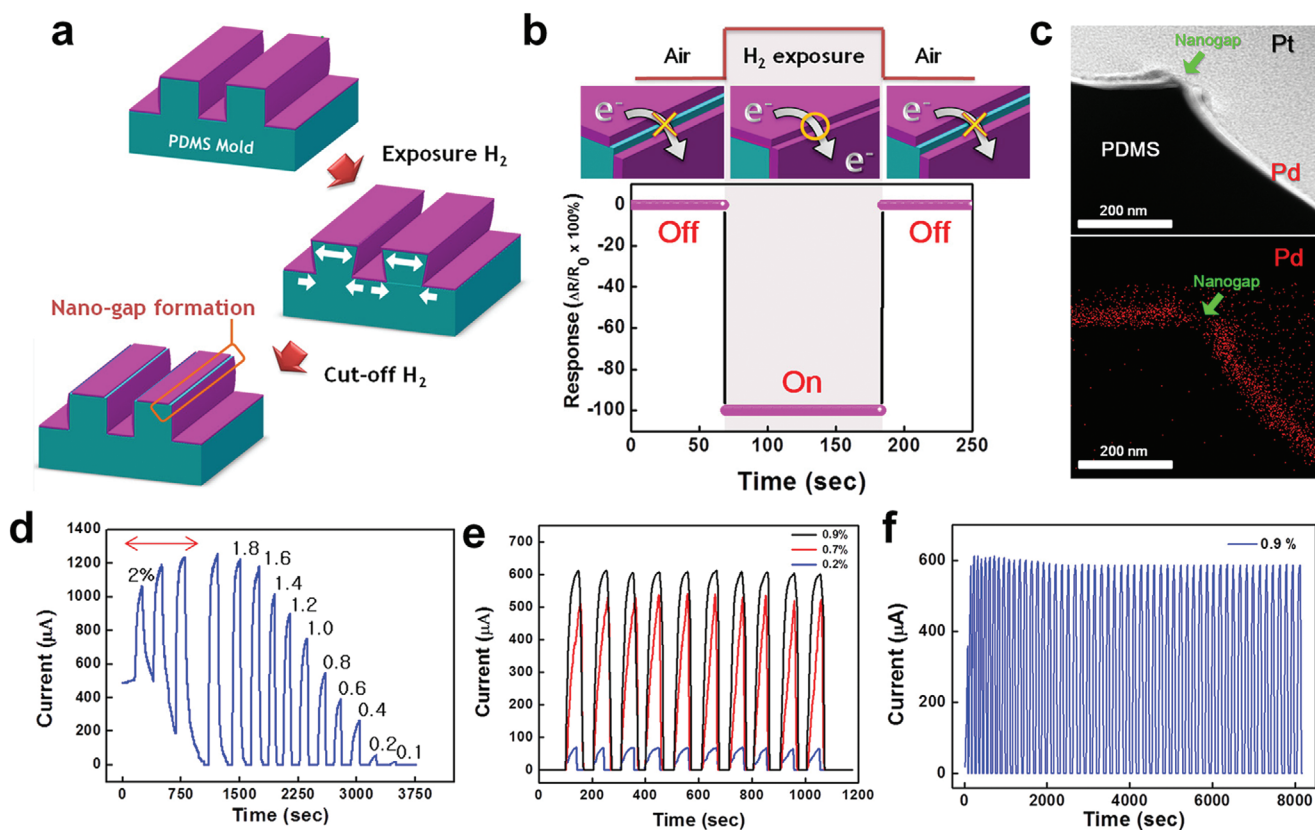
Figure 19. a) Schematic images of the mechanism for Pd nanogap formation via volumetric expansion and contraction through H_2 absorption and desorption. b) Schematic images of the sensing mechanism through the changes in current response with ON–OFF operation depending on electron transfer at the edge of the Pd/PDMS sensor. c) Cross-sectional STEM images of the edge of the Pd/PDMS sensor after H_2 cycling treatment (top) and elemental mapping images of nanogap formation (disconnected Pd layer, red dots) (bottom). d) The real-time electrical responses of a Pd/PDMS sensor at room temperature in air. Repeatability tests of the real-time electrical responses versus time of the Pd/PDMS sensor e) in the H_2 concentration ranges of 0.2–0.9% at 10 on/off cycles and f) under 0.9% H_2 concentration at 55 on/off cycles. Reproduced with permission.[42] Copyright 2015, Elsevier B.V.

4.3. Thermal Stability

As previously stated, Pd-based MOTIFE H_2 sensors have several advantages, such as low cost, easy fabrication, and high sensing performance (e.g., rapid response time and low detection limit). On the other hand, elastomeric substrates can be thermally degraded at higher temperatures. Therefore, the thermal stability of these sensors must be investigated to evaluate their commercial applicability. Here, the influence of thermal exposure on the H_2-sensing performance of the Pd MOTIFEs was examined by annealing the nanogap sensor at temperatures up to 200 °C.[47] The test sensors were prepared by thermal treatment after nanogap formation through mechanical stretching and initial H_2 cycling. **Figure 21**a shows the H_2-sensing properties of the Pd MOTIFEs annealed at different temperatures (80–200 °C). The sensing measurements were performed at room temperature. The sensor annealed at 80 °C exhibited the best sensing performance (the highest current response level and lowest detection limit of 0.5% H_2). As the annealing temperature increased above 80 °C, the sensors showed lower current levels and higher detection limits. Particularly, the sensor annealed at 200 °C showed no response in the overall H_2 concentration range. According to scanning electron microscope

(SEM) analysis, the Pd nanogap width increased linearly with an increase in the annealing temperature, as shown in Figure 21b. In addition, Pd buckling on PDMS, which is perpendicular to the nanogap direction, was generated with a shorter wavelength with an increase in the annealing temperature above 80 °C. Therefore, the decrease in the sensing current at higher annealing temperatures can be attributed to the enlarged Pd nanogap, and eventually, at 200 °C, the Pd layer is disconnected and there is no current flow.

Figure 21c shows the sensing response of the sensors annealed at 100 °C for seven cycles under exposure to 10% H_2. The results indicated that the sensor that was annealed at temperatures up to 100 °C exhibited a perfect on–off operation with a response time of less than 1 s. Figure 21d shows reproducibility tests of the real-time current responses in 10% H_2 of the sensors that were annealed at 90–150 °C. The results revealed that the response was stable without significant signal change even though the sensor performance was degraded due to thermal denaturation of the elastomeric substrate. Accordingly, this study demonstrated that the Pd-based MOTIFE can operate in a perfectly on–off mode with rapid response times (<1 s) even when the sensor was annealed at temperatures up to 100 °C.
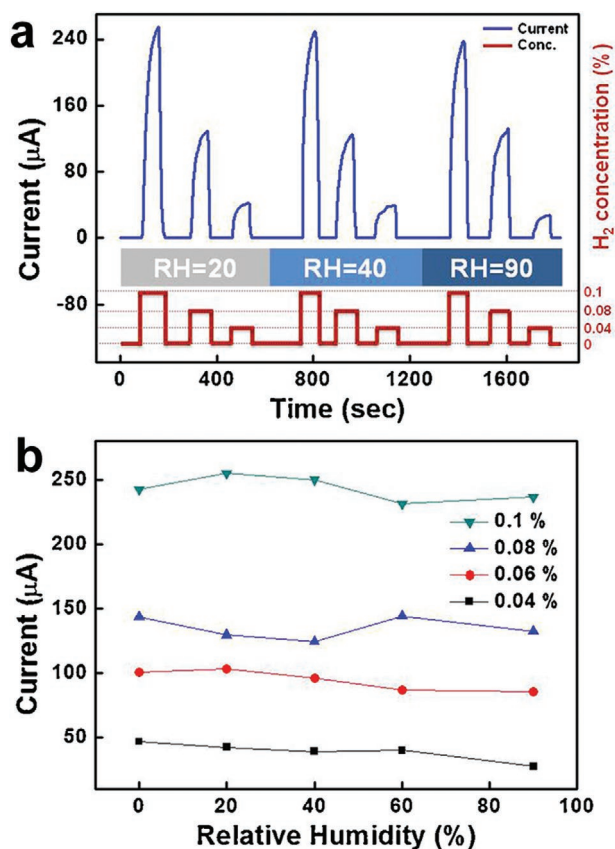
Figure 20. a) Real-time electrical responses of the Pd MOTIFEs at various relative humidity (RH), and b) their humidity dependent responses from 0% to 90% RH, for different H_2 concentrations. Reproduced with permission.[46] Copyright 2016, Elsevier B.V.

4.4. Selectivity

The selective reaction of Pd nanogap-based MOTIFEs toward H_2 has been tested for several toxic gases, such as CO, NO, NO_2, and NH_3. Various target gases were continuously injected into the sensor. 10 ppm (0.001%) of the different toxic gases were individually released into the sensor after a single cycle of 0.5% H_2 gas-in and gas-out, as shown in **Figure 22**. There was no current response to the added gases. The results indicated that the Pd MOTIFEs reacted only with H_2 gas. Furthermore, the current response level of the sensor to 0.5% H_2 remained nearly unchanged throughout all exposures of the tested toxic gases. This study demonstrated that Pd-based MOTIFEs have selective on/off responses only for H_2 and do not degrade in the presence of the tested toxic gases.

5. Performance of Pd Nanogap H_2 Sensors

5.1. Sensitivity

Sensitivity—how precisely the target can be detected—is one of the most crucial performances of a sensor. Generally, the sensitivity is defined as the ratio of the change in signal to the initial value; in the case of an electrical response, it can be obtained

from a change in electrical conductance (current) or resistance. In on–off sensors because the initial state "off" is an open circuit and the electrical conductance is zero, the sensitivity should be obtained from the resistance. Therefore, the sensitivity of MOTIFEs and CPEs were defined as $\Delta R / R_0 \times 100(\%)$, where ΔR and R_0 are the resistance change ($R - R_0$) and initial resistance, respectively.[36,37]

Figure 23 shows the sensitivity of a resistance sensor using Pd film and a CPE at various H_2 concentrations. The sensitivity of the resistance sensor based on the carrier scattering mechanism was found to be very small. This is because of the limited change in resistance caused by the H_2 absorption of the Pd film. In these "on" sensors, a sensing signal corresponding to the initial value is required to obtain high sensitivity. On the other hand, in the case of CPE, an on–off sensor because the initial resistance was infinite, a sensitivity of 100% could be easily obtained even at a negligible signal. In fact, all the Pd nanogaps on elastomer sensors, including MOTIFEs, showed 100% sensitivity irrespective of the H_2 concentration, even for signals at the detection limit.[18,36,37,41,42,44,45] This is a distinguishing feature of the on–off sensor and one of the outstanding advantages of MOTIFEs and CPEs compared to sensors with other mechanisms such as a low H_2 concentration sensor.

In the evaluation of the sensitivity of such an on–off sensor, the result may be different depending on the measurement configuration. To obtain the absolute value of the resistance in the Pd film, it is necessary to apply the 4-terminal measurement using a current source and voltage meter. However, when the open circuit of the off state is configured, an arbitrary voltage value can be obtained by the internal resistance of the measurement system, even when it has zero electrical conductance. In the typical I–V measuring system used in these works, a resistance of 100 MΩ is obtained in the open circuit rather than infinity value.[37] Furthermore, the I–V measurement that applies a fixed current can cause damage to systems with high resistance. Consequently, in MOTIFEs and CPEs, it is desirable to conduct V–I measurements using a voltage source and a current meter for H_2 detection using the electrical response.

5.2. Discernibility at High H_2 Concentrations

Another important factor in the performance of an H_2 sensor is the discernibility, which indicates how accurately the concentration of H_2 can be quantified with a scalable response.[36] In the on–off sensors MOTIFEs and CPEs, it can be determined by the range from the detection limit (at which the circuit is closed and initiates the "on" state owing to the Pd expansion) to the lowest resistance point due to completely closed nanogaps (the high concentration discernibility limit). As shown in **Figure 24**a, in both MOTFE and CPE made of pure Pd nanogaps, the discernibility limit was found to be at the H_2 concentration of 2%,[18,37] which did not change even if the nanogap width was varied by an additional process such as LNF.[38] This can be attributed to the α to β phase transition. The α-phase Pd is transformed into β Pd hydride as the H_2 concentration increases above 1%,[23] and the expansion due to
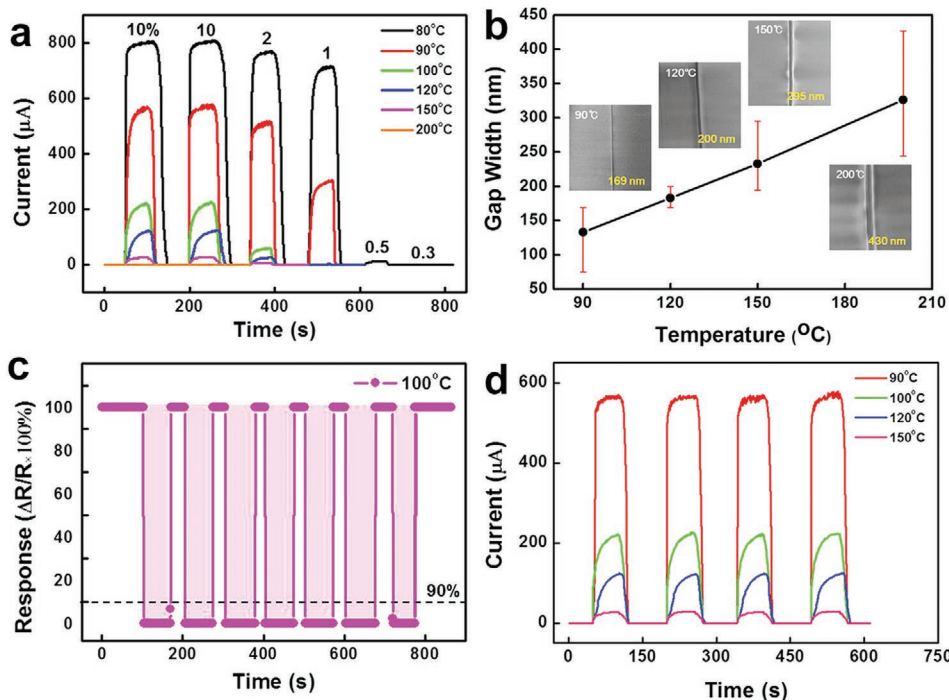
Figure 21. a) Real-time electrical responses of the Pd MOTIFEs annealed at various temperatures ranging 80–200 °C. b) Temperature dependence of the nanogap length along with the SEM images of the surface of Pd nanogaps. The red line indicates the error. c) Sensor response versus time plot of the Pd nanogap sensors annealed at 100 °C in 10% H_2. d) Reproducibility tests of the real-time electrical responses of the annealed Pd nanogap sensors in 10% H_2. Reproduced with permission.[47] Copyright 2016, Elsevier B.V.

the β phase transition, which is 3.47% of the lattice parameter, is significantly larger than that of the α phase due to the penetration of H_2 into Pd (0.13%).[69–71] As a result, the closing of the nanogaps is accelerated due to H_2 exposure, thereby rapidly increasing the change in current response. However, when the concentration of H_2 increases above 2%, exceeding the maximum H_2 solid solubility, the phase transition to the β Pd hydride is completed and the nanogaps are sufficiently closed, so that the change in the electrical response according to the increase in H_2 concentration is no longer observed.[74,75]
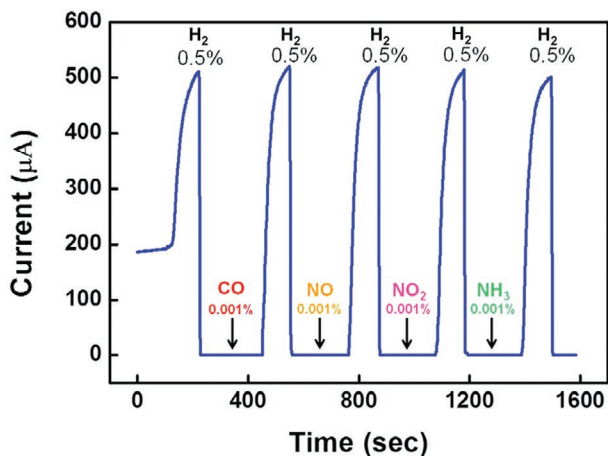

Figure 22. Real-time electrical responses of the selective H_2 response, compared with responses to other interfering gases. Reproduced with permission.[46] Copyright 2016, Elsevier B.V.

The low discernibility limit in the patterned CPE can also be attributed to the same mechanism, and the current changes according to the H_2 concentration of pure Pd in Figure 24b clearly shows the behavior described above.

On the other hand, as in the case of the PdNi alloy MOTIFE and Pd–PMMA hybrid MOTIFE, the discernibility at high concentrations can be improved through the use of different materials (Figure 24a).[36,41] In particular, by alloying Ni with Pd, it was possible to achieve an enhancement in H_2 solid solubility to more than 10%, which is more than five times the value for pure Pd. This can be attributed to the suppression of the α to β phase transition due to Ni inclusions, resulting in an increase in the H_2 concentration at which the β Pd hydride is completely formed.[76,77] Therefore, as the response trend of the PdNi alloys with different Ni compositions shows in Figure 24b, there is room for further improvement of the discernibility by increasing the Ni content.[36] However, it was found that the excessive increase in the Ni content caused a decrease in the sensitivity by increasing the resistance of Pd film,[65] causing a corresponding deterioration in the detection limit because of the reduction in H_2 solubility and the decrease in the volume expandability of Pd.[78]

5.3. Response Time

Next, the response times of H_2 detection using MOTIFEs and CPEs are summarized. The response time is as important as sensitivity and discernibility in the commercial application of a sensor, and it can be determined by dividing the response
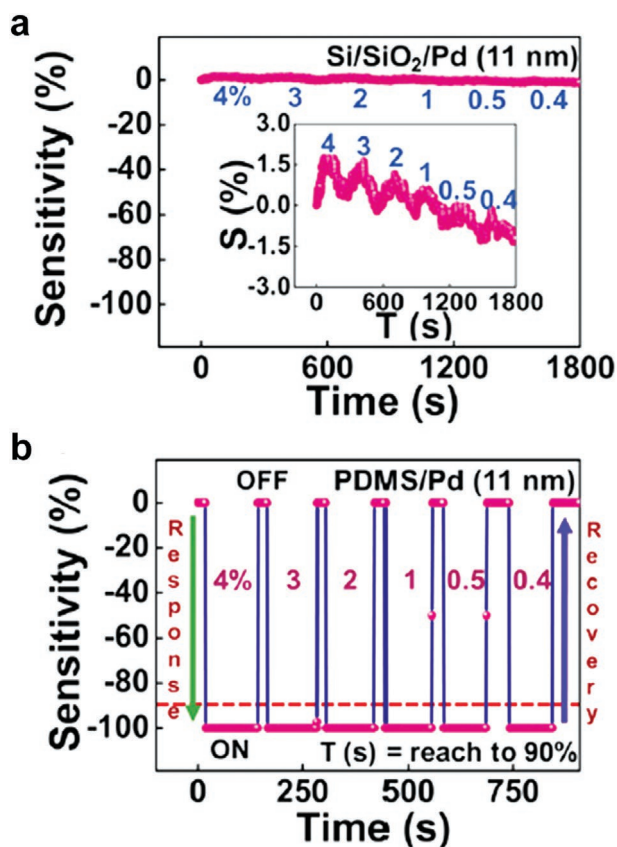
**ADVANCED
SCIENCE NEWS**

www.advancedsciencenews.com

**ADVANCED
MATERIALS**

www.advmat.de

Figure 23. The real-time sensitivity of a) a resistance sensor made of Pd film on the Si substrate and b) a CPE with Pd nanogaps on the PDMS substrate, at various H_2 concentrations. The inset of (a) is a magnified image of the plot to illustrate the sensitivity. Reproduced with permission.[37] Copyright 2012, Elsevier B.V.

above because of the measurement interval of 1 s, except for the case of typical MOTIFE with 0.42 s intervals. However, as shown in Figure 25a, it can be inferred from the 100% sensitivity obtained within the measurement interval (1 s) that the response and recovery times were much shorter than 1 s. The patterned CPE also showed response and recovery within 1 s in 0.1% to 2% H_2 concentrations.[42] The fastest responses were obtained from the Pd–PMMA hybrid MOTIFE. The real-time electrical response was obtained at 0.4 s intervals at 2% concentration of H_2 exposure, and the response and recovery times were reported as ≈0.36 s (Figure 25b).[41] The response and recovery times, which are ≈100 times faster than those obtained in Pd films on silicon substrates (64 s),[18] were attributed to the highly mobile Pd film on the elastomeric PDMS substrate, and were evaluated to be sufficient for commercial needs.
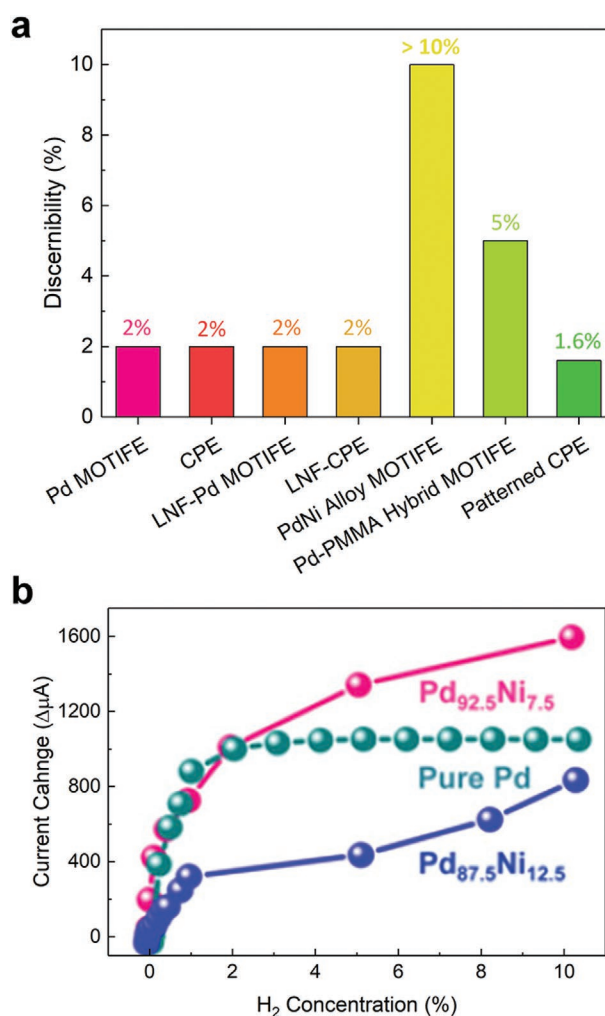

Figure 24. a) The limitation of high H_2 concentration discernibility in various MOTIFEs and CPEs. The discernibility limit data of Pd MOTIFE,[18] CPE,[37] LNF-Pd MOTIFE,[38] LNF-CPE,[38] PdNi alloy MOTIFE,[36] Pd–PMMA hybrid MOTIFE,[41] and patterned CPE[42] were obtained from previous works. b) The change in electrical response of Pd and PdNi alloy MOTIFEs as a function of H_2 concentration from 0% to 10%. Reproduced with permission.[36] Copyright 2012, Elsevier B.V.
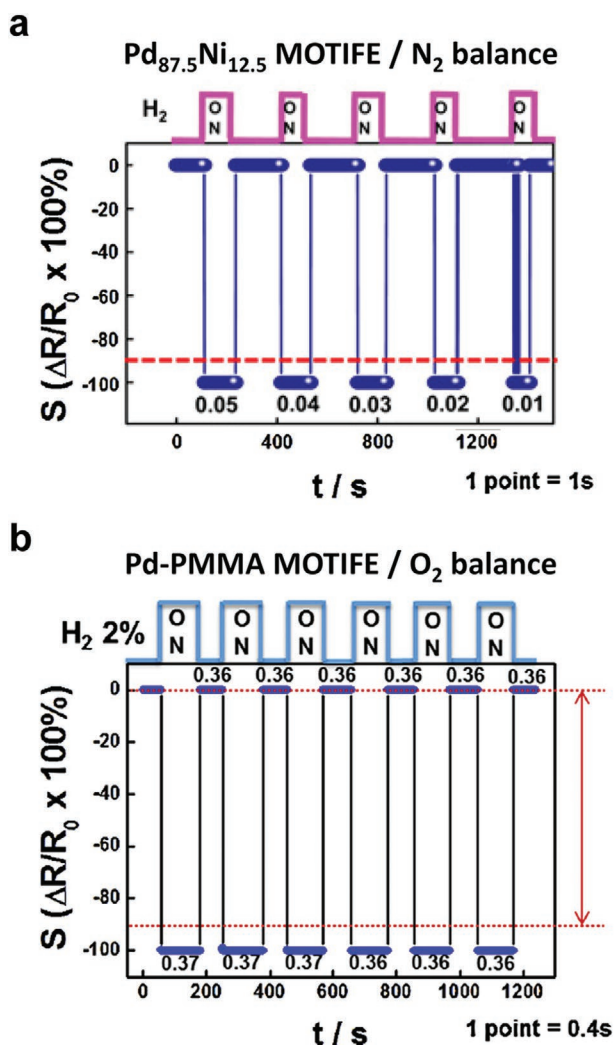
time, which is the reaction speed when exposed to H_2, and the recovery time, which is the time to return to its original state when H_2 is removed. The response time is defined as the time to reach 90% of the total change in the electrical signal, and the recovery time is determined as the time to recover by 90%, that is, the time to return to a sensitivity of 10%.[18,44] Therefore, these properties can be obtained from real-time sensitivity, as shown in **Figure 25**.

In almost all MOTIFEs and CPEs, the response and recovery times were found to be ≈1 s, regardless of H_2 concentration, and the recovery time was slightly longer than the response time in general.[18,36–38,41,42] The response time of the typical MOTIFE was obtained as 0.67 s at 2% H_2 concentration, and the recovery time was 3.36 s.[18] In a typical CPE, a time of less than 1 s was obtained not only in the response but also in the recovery in the H_2 range of 0.4% to 4%.[37] It was confirmed that such short response and recovery times were maintained even when the detection limit was reduced using the LNF process.[38] In the case of PdNi alloy MOTIFEs, response and recovery times of less than 1 s were obtained even at a low H_2 concentration of 0.02% to 0.05%.[36] However, to analyze accurate response and recovery times, a much shorter measurement interval is required. Therefore, values of less than 1 s could not be analyzed accurately in the results

ADVANCED
SCIENCE NEWS

www.advancedsciencenews.com

ADVANCED
MATERIALS

www.advmat.de

Figure 25. a) The real-time sensitivity of a PdNi alloy MOTIFE with various H_2 concentrations in N_2 carrier. The numbers 0.05 to 0.01 indicate the H_2 concentrations (in %), and the time interval between data points is 1 s. Reproduced with permission.[36] Copyright 2012, Elsevier B.V. b) The real-time sensitivity of a Pd–PMMA hybrid MOTIFE with a constant H_2 concentration of 2% in air atmosphere. The lower and upper numbers in the graph represent response and recovery times, respectively. The time interval is 0.4 s. Reproduced with permission.[41] Copyright 2014, Elsevier B.V.

6. Summaries and Future Outlook

We have discussed recent advances in the development of Pd nanogap-based hydrogen gas (H_2) sensors supported on elastomeric substrates, which have been achieved over the past decade. Since Pd-based H_2 sensors operating in an on–off manner—a new paradigm in H_2 gas detection enabled by the formation of Pd nanogaps—were introduced using Pd mesowire arrays, much effort has been made to improve H_2-sensing performance to meet the requirements of practical applications. Pd nanogap-based sensors, which operate with a gap opening and closing mechanism, typically have many advantages, such as very high sensitivity and reliability and rapid response, compared to conventional Pd-based sensors operated by electron scattering mechanisms. However, these sensors also have some

disadvantages, such as complicated fabrication processes and poor low detection limits, which need to be solved out. Among various approaches to obtain enhanced sensing properties, better reliability, and easier manufacturing processes, the use of an elastomeric substrate has provided a new methodological paradigm to overcome the disadvantages of Pd nanogap-based sensors.

Controlling the width of nanogaps, which is one of main challenging issues in the use of these sensors utilizing Pd nanogaps on an elastomeric substrate, has been attempted in Pd MOTIFE. The nanogaps in Pd MOTIFEs are created as a result of Pd film shrinkage after mechanical stretching and internal stress relaxation after H_2 removal. In order to reduce the nanogap width to less than 100 nm in Pd MOTIFEs, in which the low detection limit is good enough, various methods have been attempted. 1) Adding a small amount of Ni to Pd can effectively reduce the nanogap width to sub-100 nm. The reduced width of the nanogap in Pd–Ni film on an elastomeric substrate is due to the increased fracture toughness and ductility resulting from the material properties of Ni, which exhibits higher toughness and ductility than Pd (Pd–Ni alloy MOTIFE). 2) Sub-100 nm nanogaps were also obtained using an LNF of Pd-sputtered elastomeric substrates due to the thermal contraction of cracked Pd film. This is attributed to the difference in the coefficient of thermal expansion between the Pd film and the PDMS (LNF-Pd MOTIFE). 3) Extremely narrow (sub-10 nm) nanogaps in Pd MOTIFE were achieved by the combination of tensile straining and the fine control of the initial hydrogen concentration. The nanogap width has been shown to decrease with decreasing the H_2 concentration of the initial exposure. This is because as the H_2 concentration deceases, the amount of stress stored in the film during the expansion of the Pd film decreases (initial H_2-engineered Pd MOTIFE). 4) A strain engineering method produced nanogaps in Pd MOTIFE parallel as well as vertical to the straining direction at higher velocities and magnitudes of tensile strain. A significant reduction in the detection limit to 50 ppm in air was observed, which was due to a decrease in the nanogap width and an increase in the nanogap density. Thus, the nanogap density also becomes an important factor affecting the detection limit (strain-engineered Pd MOTIFE).

The reliability in ambient atmosphere, stability under humidity conditions, thermal stability, and selectivity in several toxic gases have been extensively investigated for practical applications of Pd MOTIFEs. To improve the reliability of a Pd MOTIFE in ambient atmosphere, a PMMA filter layer was applied to prevent from interference of O_2 and H_2O in air during H_2 sensing. The Pd–PMMA hybrid nanogap sensor operates well as an on–off sensor and shows a significant improvement in detection limit in air. In addition, the interference of humidity and thermal exposure on the H_2-sensing performance of Pd MOTIFEs was investigated, revealing that the sensing performance of the Pd-based MOTIFEs does not significantly degrade even under high RH conditions (90%) and a Pd MOTIFE can operate in a perfectly on–off mode with rapid response times (<1 s) even annealed at temperatures up to 100 °C. More importantly, it was found that the Pd MOTIFEs have selective on/off responses only for H_2 and they exhibit no degradation due to the tested toxic gases, specifically CO, NO,

**ADVANCED
SCIENCE NEWS**

www.advancedsciencenews.com

**ADVANCED
MATERIALS**

www.advmat.de

NO$_2$, and NH$_3$. In addition, the Pd MOTIFE based on–off sensors generally showed 100% sensitivity and 1 s response and recovery times.

Significant advances have been made on Pd nanogap H$_2$ sensors using an elastomeric substrate, demonstrating the potential to provide an optimal sensor by achieving several important functions, such as easy fabrication, low detection limit, high sensitivity, high discernibility, rapid response, good reliability, and good stability in humid and thermal conditions. However, there are still some issues, such as reliability for operation in the wide temperature range –40 to 200 °C and stability for long-term use for practical applications, in particular, which are crucial in the use of hydrogen fuel cell vehicles. New insights, approaches, or converging technologies in various research fields are necessary to overcome existing shortcomings and facilitate the realization of Pd MOTIFEs for commercial applications in the near future.

Conflict of Interest

The authors declare no conflict of interest.

[1] T. Hübert, L. Boon-Brett, G. Black, U. Banach, *Sens. Actuators, B* **2011**, *157*, 329.

[2] P. J. Shaver, *Appl. Phys. Lett.* **1967**, *11*, 255.

[3] I. Lundström, S. Shivaraman, C. Svensson, L. Lundkvist, *Appl. Phys. Lett.* **1975**, *26*, 55.

[4] W. Shin, M. Matsumiya, N. Izu, N. Murayama, *Sens. Actuators, B* **2003**, *93*, 304.

[5] K. Ito, T. Ohgami, *Appl. Phys. Lett.* **1992**, *60*, 938.

[6] B. S. Kang, F. Ren, B. P. Gila, C. R. Abernathy, S. J. Pearton, *Appl. Phys. Lett.* **2004**, *84*, 1123.

[7] J. Kong, M. G. Chapline, H. Dai, *Adv. Mater.* **2001**, *13*, 1384.

[8] M. Yun, N. V. Myung, R. P. Vasquez, C. Lee, E. Menke, R. M. Penner, *Nano Lett.* **2004**, *4*, 419.

[9] P. Pandey, J. K. Srivastava, V. N. Mishra, R. Dwivedi, *Solid State Sci.* **2009**, *11*, 1370.

[10] D. Luna-Moreno, D. Monzón-Hernández, J. Villatoro, G. Badenes, *Sens. Actuators, B* **2007**, *125*, 66.

[11] R. C. Hughes, W. K. Schubert, R. J. Buss, *J. Electrochem. Soc.* **2019**, *142*, 249.

[12] Y. Im, C. Lee, R. P. Vasquez, M. A. Bangar, N. V. Myung, E. J. Menke, R. M. Penner, M. Yun, *Small* **2006**, *2*, 356.

[13] K. Baba, U. Miyagawa, K. Watanabe, Y. Sakamoto, T. B. Flanagan, *J. Mater. Sci.* **1990**, *25*, 3910.

[14] L. Huang, H. Gong, D. Peng, G. Meng, *Thin Solid Films* **1999**, *345*, 217.

[15] S. H. Lim, B. Radha, J. Y. Chan, M. S. Saifullah, G. U. Kulkarni, G. W. Ho, *ACS Appl. Mater. Interfaces* **2013**, *5*, 7274.

[16] S. Walia, R. Gupta, K. D. Rao, G. U. Kulkarni, *ACS Appl. Mater. Interfaces* **2016**, *8*, 23419.

[17] R. Gupta, A. A. Sagade, G. U. Kulkarni, *Int. J. Hydrogen Energy* **2012**, *37*, 9443.

[18] J. Lee, W. Shim, E. Lee, J. S. Noh, W. Lee, *Angew. Chem., Int. Ed. Engl.* **2011**, *50*, 5301.

[19] F. Favier, E. C. Walter, M. P. Zach, T. Benter, R. M. Penner, *Science* **2001**, *293*, 2227.

[20] R. M. Penner, *Acc. Chem. Res.* **2017**, *50*, 1902.

[21] F. Yang, D. K. Taggart, R. M. Penner, *Small* **2010**, *6*, 1422.

[22] X. Li, Y. Liu, J. C. Hemminger, R. M. Penner, *ACS Nano* **2015**, *9*, 3215.

[23] F. A. Lewis, *The Palladium Hydrogen System*, Academic Press, London **1967**.

[24] O. Dankert, A. Pundt, *Appl. Phys. Lett.* **2002**, *81*, 1618.

[25] G. Kaltenpoth, P. Schnabel, E. Menke, E. C. Walter, M. Grunze, R. M. Penner, *Anal. Chem.* **2003**, *75*, 4756.

[26] M. Ramanathan, G. Skudlarek, H. H. Wang, S. B. Darling, *Nanotechnology* **2010**, *21*, 125501.

[27] T. Kiefer, L. G. Villanueva, F. Fargier, F. Favier, J. Brugger, *Appl. Phys. Lett.* **2010**, *97*, 121911.

[28] T. Xu, M. P. Zach, Z. L. Xiao, D. Rosenmann, U. Welp, W. K. Kwok, G. W. Crabtree, *Appl. Phys. Lett.* **2005**, *86*, 203104.

[29] E. C. Walter, F. Favier, R. M. Penner, *Anal. Chem.* **2002**, *74*, 1546.

[30] F. Yang, D. K. Taggart, R. M. Penner, *Nano Lett.* **2009**, *9*, 2177.

[31] V. L. Ferrara, B. Alfano, E. Massera, G. D. Francia, *IEEE Trans. Nanotechnol.* **2008**, *7*, 776.

[32] M. Z. Atashbar, S. Singamaneni, *Sens. Actuators, B* **2005**, *111*, 13.

[33] S. Cherevko, N. Kulyk, J. Fu, C.-H. Chung, *Sens. Actuators, B* **2009**, *136*, 388.

[34] K. Kyun Tae, S. Jun, C. S. Min, *IEEE Sens. J.* **2006**, *6*, 509.

[35] T. Kiefer, A. Salette, L. G. Villanueva, J. Brugger, *J. Micromech. Microeng.* **2010**, *20*, 105019.

[36] E. Lee, J. Lee, J.-S. Noh, W. Kim, T. Lee, S. Maeng, W. Lee, *Int. J. Hydrogen Energy* **2012**, *37*, 14702.

[37] J. Lee, J.-S. Noh, S. H. Lee, B. Song, H. Jung, W. Kim, W. Lee, *Int. J. Hydrogen Energy* **2012**, *37*, 7934.

[38] T. Chang, H. Jung, B. Jang, J. Lee, J.-S. Noh, W. Lee, *Sens. Actuators, A* **2013**, *192*, 140.

[39] H. Jung, B. Jang, W. Kim, J.-S. Noh, W. Lee, *Sens. Actuators, B* **2013**, *178*, 689.

[40] Y. T. Lee, H. Jung, S. H. Nam, P. J. Jeon, J. S. Kim, B. Jang, W. Lee, S. Im, *Nanoscale* **2013**, *5*, 8915.

[41] B. Jang, K. Y. Lee, J.-S. Noh, W. Lee, *Sens. Actuators, B* **2014**, *193*, 530.

[42] B. Jang, S. Cho, C. Park, H. Lee, M.-J. Song, W. Lee, *Sens. Actuators, B* **2015**, *221*, 593.

[43] Y. Pak, N. Lim, Y. Kumaresan, R. Lee, K. Kim, T. H. Kim, S. M. Kim, J. T. Kim, H. Lee, M. H. Ham, G. Y. Jung, *Adv. Mater.* **2015**, *27*, 6945.

[44] S. Kim, B. Jang, J. Park, Y.-K. Lee, H.-S. Lee, S. Cho, W. Lee, *Sens. Actuators, B* **2016**, *230*, 367.

[45] S. Kim, H.-S. Lee, B. Jang, S. Cho, W. Lee, *J. Mater. Sci.* **2016**, *51*, 4530.

[46] W. Kim, B. Jang, H.-S. Lee, W. Lee, *Sens. Actuators, B* **2016**, *224*, 547.

[47] B. Jang, W. Kim, M.-J. Song, W. Lee, *Sens. Actuators, B* **2017**, *240*, 186.

[48] Y. Pak, Y. Jeong, N. Alaal, H. Kim, J. Chae, J.-W. Min, A. A. S. Devi, S. Mitra, D. H. Lee, Y. Kumaresan, W. Park, T.-W. Kim, I. S. Roqan, G.-Y. Jung, *Adv. Mater. Interfaces* **2019**, *6*, 1801442.

[49] J. Lee, M. Chung, K. Choi, J. Yoo, J. Yoon, in *2019 IEEE 32nd Int. Conf. on Micro Electro Mechanical Systems (MEMS)*, IEEE, Piscataway, NJ **2019**, pp. 496–499, https://doi.org/10.1109/MEMSYS.2019.8870836.

[50] B. Sakintuna, F. Lamari-Darkrim, M. Hirscher, *Int. J. Hydrogen Energy* **2007**, *32*, 1121.

[51] N. C. Smythe, J. C. Gordon, *Eur. J. Inorg. Chem.* **2010**, *2010*, 509.

[52] S.-i. Orimo, Y. Nakamori, J. R. Eliseo, A. Züttel, C. M. Jensen, *Chem. Rev.* **2007**, *107*, 4111.

[53] R. Griessen, A. Driessen, *Phys. Rev. B* **1984**, *30*, 4372.

[54] A. Züttel, M. Hirscher, B. Panella, K. Yvon, S.-i. Orimo, B. Bogdanović, M. Felderhoff, F. Schüth, A. Borgschulte, S. Goetze, S. Suda, M. T. Kelly, *Hydrogen as a Future Energy Carrier*, Wiley-VCH GmbH, Weinheim, Germany **2008**.

[55] P. Ferrin, S. Kandoi, A. U. Nilekar, M. Mavrikakis, *Surf. Sci.* **2012**, *606*, 679.

[56] K. Hermann, *Crystallography and Surface Structure*, Wiley-VCH GmbH, Weinheim, Germany **2011**.

[57] H. Akiba, M. Kofu, H. Kobayashi, H. Kitagawa, K. Ikeda, T. Otomo, O. Yamamuro, *J. Am. Chem. Soc.* **2016**, *138*, 10238.

[58] R. Caputo, A. L. I. Alavi, *Mol. Phys.* **2003**, *101*, 1781.

[59] A. Maeland, T. B. Flanagan, *Platinum Met. Rev.* **1966**, *10*, 20.

[60] M. J. Owen, P. J. Smith, *J. Adhes. Sci. Technol.* **1994**, *8*, 1063.

[61] D. Fuard, T. Tzvetkova-Chevolleau, S. Decossas, P. Tracqui, P. Schiavone, *Microelectron. Eng.* **2008**, *85*, 1289.

[62] M. Schlesinger, M. Paunovic, *Modern Electroplating*, Wiley, New York **2010**, p. 327.

[63] S. Kamran, K. Chen, L. Chen, *Phys. Rev. B* **2009**, *79*, 024106.

[64] H. Peisl, in *Hydrogen in Metals I: Basic Properties* (Eds: G. Alefeld, J. Völkl), Springer, Berlin **1978**, p. 53.

[65] J. C. Barton, J. A. S. Green, F. A. Lewis, *Trans. Faraday Soc.* **1966**, *62*, 960.

[66] E. J. Smythe, M. D. Dickey, G. M. Whitesides, F. Capasso, *ACS Nano* **2009**, *3*, 59.

[67] W. W. Tooley, S. Feghhi, S. J. Han, J. Wang, N. J. Sniadecki, *J. Micromech. Microeng.* **2011**, *21*, 054013.

[68] F. C. Nix, D. MacNair, *Phys. Rev.* **1942**, *61*, 74.

[69] F. L. Chen, M. Furukawa, Y. Sakamoto, *J. Less-Common Met.* **1989**, *155*, 173.

[70] H. C. Jamieson, G. C. Weatherly, F. D. Manchester, *J. Less-Common Met.* **1976**, *50*, 85.

[71] S. Wagner, H. Uchida, V. Burlaka, M. Vlach, M. Vlcek, F. Lukac, J. Cizek, C. Baehtz, A. Bell, A. Pundt, *Scr. Mater.* **2011**, *64*, 978.

[72] F. Yang, S.-C. Kung, M. Cheng, J. C. Hemminger, R. M. Penner, *ACS Nano* **2010**, *4*, 5233.

[73] S. Kumar, A. Sharma, B. Tripathi, S. Srivastava, S. Agrawal, M. Singh, K. Awasthi, Y. K. Vijay, *Micron* **2010**, *41*, 909.

[74] E. Lee, J. M. Lee, J. H. Koo, W. Lee, T. Lee, *Int. J. Hydrogen Energy* **2010**, *35*, 6984.

[75] J. S. Noh, J. M. Lee, W. Lee, *Sensors* **2011**, *11*, 825.

[76] Y.-T. Cheng, Y. Li, D. Lisi, W. M. Wang, *Sens. Actuators, B* **1996**, *30*, 11.

[77] E. Lee, J. M. Lee, E. Lee, J.-S. Noh, J. H. Joe, B. Jung, W. Lee, *Thin Solid Films* **2010**, *519*, 880.

[78] M. Shamsuddin, *J. Less-Common Met.* **1989**, *154*, 285.

Hyun-Sook Lee is a research professor of the Nano Device Laboratory in the Department of Materials Science and Engineering at Yonsei University, Korea. She received a Ph.D. degree in physics at POSTECH in 2008. Her research interests are in various materials related to high-temperature superconductors, solid-state hydrogen storages, rare-earth/rare-earth-free permanent magnets, nanostructured metal oxide semiconductor gas sensors, and Pd-based hydrogen sensors.

Jeongmin Kim is a senior researcher of the Division of Nanotechnology at DGIST in Korea. He obtained his B.S. degree in metallurgical engineering from Yonsei University in Korea. After receiving his Ph.D. degree in material science and engineering at Yonsei University, he worked as a postdoctoral researcher at UC San Diego and a research professor at Yonsei University. Throughout this time, his prime focus of research has been on 1D and 2D structures to study and enhance the material properties for applications as sensors and energy materials.

**ADVANCED
SCIENCE NEWS**

www.advancedsciencenews.com

**ADVANCED
MATERIALS**

www.advmat.de

Hongjae Moon received a Bachelor's degree in materials science and engineering from Yonsei University in 2012. He is currently a Ph.D. candidate at the Department of Materials Science and Engineering in Yonsei University under the supervision of Prof. Wooyoung Lee. He is currently studying on the low-dimensional materials for applications as sensors and energy materials.

Wooyoung Lee is a professor of the Department of Materials Science and Engineering and the Director of the Center for Super Critical Material Industrial Technology (MOTIE) at Yonsei University in Korea. He received a Ph.D. degree in physics from the University of Cambridge, United Kingdom, in 2000. He is a regular member of the National Academy of Engineering of Korea. His research interests have centered on hydrogen sensors, various metal oxide semiconducting gas sensors, and thermoelectric materials and devices.